Chem Soc Rev

REVIEW ARTICLE

View Article Online
View Journal | View Issue

Cite this: *Chem. Soc. Rev.*, 2015, 44, 4769

Fluorometric imaging methods for palladium and platinum and the use of palladium for imaging biomolecules

Matthew P. Tracey, Dianne Pham and Kazunori Koide*

Received 27th September 2014

DOI: 10.1039/c4cs00323c

www.rsc.org/csr

Neither palladium nor platinum is an endogenous biological metal. Imaging palladium in biological samples, however, is becoming increasingly important because bioorthogonal organometallic chemistry involves palladium catalysis. In addition to being an imaging target, palladium has been used to fluorometrically image biomolecules. In these cases, palladium species are used as imaging-enabling reagents. This review article discusses these fluorometric methods. Platinum-based drugs are widely used as anticancer drugs, yet their mechanism of action remains largely unknown. We discuss fluorometric methods for imaging or quantifying platinum in cells or biofluids. These methods include the use of chemosensors to directly detect platinum, fluorescently tagging platinum-based drugs, and utilizing post-labeling to elucidate distribution and mode of action.

1. Palladium imaging methods

1.1 Introduction

Palladium is a widely used transition metal in synthetic,[1] medicinal,[2] and bioorthogonal organometallic (BOOM) chemistry.[3] Its use in synthesis is highlighted by the ability to form new carbon–carbon or carbon–heteroatom bonds through palladium-catalyzed reactions, such as Kumada,[4] Suzuki–Miyaura,[5] Negishi,[6] Heck,[7] Sonogashira,[8] Buchwald–Hartwig,[9] Stille couplings,[10] Tsuji–Trost alkylation,[11] C–H functionalizations,[12,13] among others. Palladium was used as part of a drug-delivery vehicle[14] and has been rarely used in biomedical research. The metal has been used in BOOM methodologies in recent years to unmask bioactive compounds upon the addition of palladium. Thus, intracellular palladium is emerging as an exogenous metal that is of interest for those involved in BOOM chemistry and drug delivery.

Though many methods, such as inductively coupled plasma mass spectrometry (ICP-MS) and atomic absorption spectroscopy (AAS), quantify or detect heavy metals such as palladium, they are not accessible to most chemists. To alleviate this, new fluorometric and colorimetric detection methods have been developed.[15–58] These methods are often difficult to translate to intracellular environments, due to toxic components or biologically incompatible reagents for detection. As such, imaging methods for palladium in biological samples remain underdeveloped. Methods such as a

Department of Chemistry, University of Pittsburgh, 219 Parkman Avenue, Pittsburgh, Pennsylvania 15260, USA. E-mail: koide@pitt.edu

Matthew P. Tracey

Matthew P. Tracey earned his BSc in Chemistry at Fordham University in 2011. While there, he researched dendrimer synthesis and applications under Professor Amy Balija. He is currently a PhD student at the University of Pittsburgh, studying development of new fluorescence-based approaches for metal detection and new synthetic methods under the auspices of Professor Kazunori Koide.

Dianne Pham

Dianne Pham earned her BSc in Chemistry and Mathematics at Carlow University in 2011. She entered the University of Pittsburgh in 2012 as a PhD student. Her research interests include detection of biologically relevant molecules and mechanisms of spliceosome inhibition as related to disease progression. She studies under the guidance of Professor Kazunori Koide.

palladium-based DNA detection method are innovative and inspiring;[59] nonetheless, this review will primarily focus on the use of palladium as an imaging agent or the target metal in live cells.

Methods for engineering palladium's synthetic utility in biological environments are an emerging field, relying on water-compatible palladium-catalyzed reactions to form bioactive compounds. Using either palladium salts uptaken into cells or palladium microspheres, a fluorescent molecule can be cross-coupled with a targeting moiety to image organelles of interest.[60] Additionally, palladium can be used to conjugate a protein of interest with a fluorophore or other imaging moiety.[3,61,62] Recent seminal works have shown that not only can palladium be used in this manner, but it can do so with less toxic reagents than the copper-catalyzed azide–alkyne Hüisgen cycloaddition.[61–64]

1.2 Imaging palladium *in vitro* and *in vivo*

In 2010, Ahn and coworkers reported the first live cell imaging of palladium using the alkyne-based chemodosimeter **1**, which was used in zebrafish.[65] Alkylation of the phenol suppressed fluorescence of Pittsburgh Green. Exposure to $PdCl_2$ cleaved the propargylic ether bond, thereby restoring the fluorescence emitted from Pittsburgh Green (Scheme 1).

Chemodosimeter **1** is the first fluorogenic compound used for palladium imaging *in vivo*; zebrafish were exposed to aqueous $PdCl_2$ (0, 5, 10, 20 μM) and **1** (20 μM) at 28 °C. Fluorescence microscopy showed increased fluorescence inside the zebrafish correlating to palladium concentrations (Fig. 1). Validation of the experiment appears to have been omitted to show that palladium species, and not the secondary effects for the addition of palladium, induced fluorescence in zebrafish.[65]

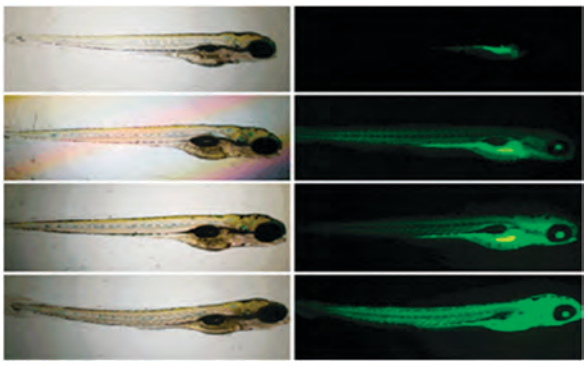

Fig. 1 Five-day-old zebrafish incubated with 20 μM alkyne **1** and various concentrations 0, 5, 10, and 20 μM $PdCl_2$. Left: phase contrast image. Right: fluorescence microscopic image. Reproduced from *Chem. Commun.*, 2010, **46**, 3964–3966 with permission from The Royal Society of Chemistry. Copyright 2010.

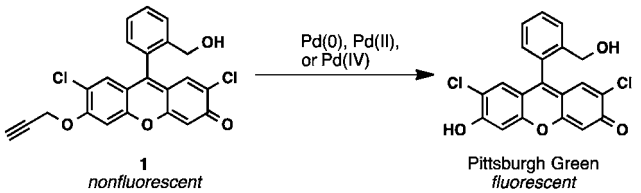

Scheme 1 Exposure of **1** to palladium releases fluorescent Pittsburgh Green.[65]

Kazunori Koide

Professor Koide obtained his bachelor's and master's degrees from the Department of Pharmaceutical Sciences at the University of Tokyo, and a PhD in chemistry at the University of California, San Diego, under the guidance of Professor K. C. Nicolaou. He conducted post-doctoral research with Professor Gregory L. Verdine in the Department of Chemistry and Chemical Biology at Harvard University. He then began his independent career in the Department of Chemistry at the University of Pittsburgh. His current research interests include development of new synthetic methods, total synthesis and chemical biology of natural products, and development and applications of fluorescent chemosensors.

In 2011, Du, Zhang, and coworkers disclosed a method for imaging palladium in macrophages using the alkyne-based ratiometric chemodosimeter, **2**.[66] When exposed to palladium, the propargylic ether bond was cleaved, and the released phenol emission shifted from 480 nm to 553 nm after excitation at 364 nm due to increased electron donation from the oxygen atom. Exposure of chemodosimeter **2** to palladium ions of various oxidation states generated a green fluorescent emission at 553 nm with an isosbestic point at 391 nm (Scheme 2). As an imaging agent, RAW 264.7 macrophage cells were incubated with 5 mM **2** following exposure to 40 mM $PdCl_2$. Increased fluorescence indicated the utility of **2** for imaging palladium (Fig. 3).

During resubmission for this manuscript, a colorimetric and ratiometric naphthalamide-based probe was disclosed (Fig. 3).[67]

Goswami and coworkers disclosed a colorimetric and fluorimetric bio-imaging method for palladium using the nitrile-based chemodosimeter **4**.[39] The cyano group of **4** disrupts the conjugation system of rhodamine 6G. Addition of Pd(II) removed the cyano group from chemodosimeter **4**, restoring the fluorescence at 555 nm upon excitation at 505 nm (Scheme 3).[39] This method also has utility as a colorimetric detection method based on the color of rhodamine 6G.[39]

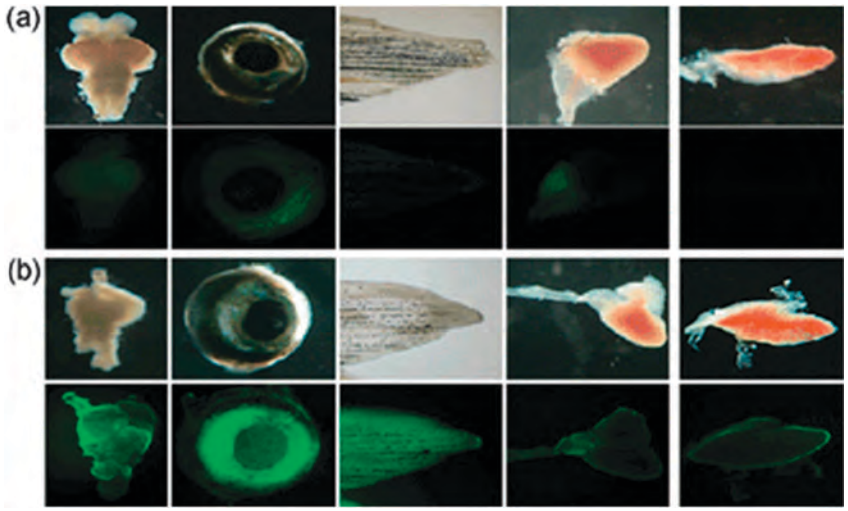

Fig. 2 Images of adult zebrafish organs treated with 20 μM alkyne **1** after incubation (a) without $PdCl_2$ or (b) with 500 nM $PdCl_2$. Top: phase contrast images; bottom: fluorescence microscopic images. Adult zebrafish were exposed to 500 nM $PdCl_2$ in E3 embryo media for 24 h at 28 °C and then incubated with 20 μM alkyne **1** for 30 min at 28 °C. Reproduced from reproduced from *Chem. Commun.*, 2010, **46**, 3964–3966 with permission from The Royal Society of Chemistry. Copyright 2010.

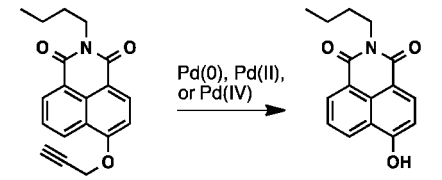

2
Emission: 480 nm

3
Emission: 553 nm

Scheme 2 Exposure of ratiometric chemodosimeter **2** to various palladium oxidation states cleaved the propargylic ether and shifted the emission wavelength from 480 nm to 553 nm.[66]

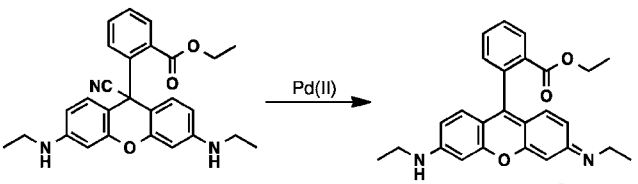

4
nonfluorescent

Scheme 3 Exposure of nitrile **4** to Pd(II) cleaves the C–CN bond and releases fluorescent rhodamine 6G.

Nitrile **4** was tested in HeLa cells for membrane permeability and utility as a bio-imaging reagent for palladium. Cells were incubated first with 50 μM $PdCl_2$ followed by 50 μM chemodosimeter **4**. Only cells incubated with both showed an increased emission signal in the red channel by fluorescence imaging.[39] Nuclear staining with DAPI indicated that the fluorescence was localized in the cytoplasm (Fig. 4).[39] This result indicates that cleavage of a C–CN bond can be utilized to image intracellular palladium.

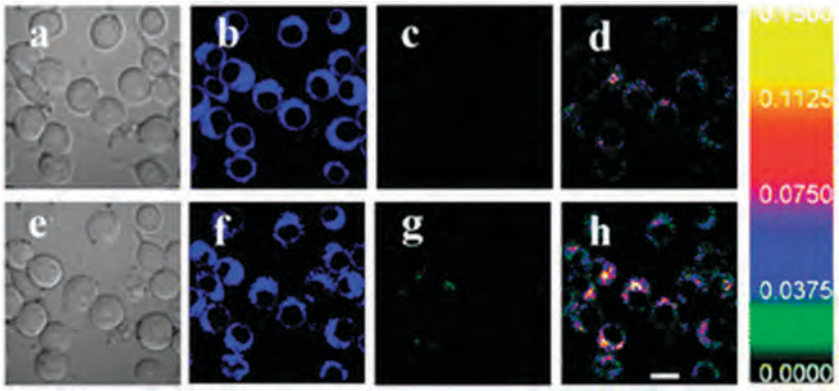

Fig. 3 Confocal fluorescence images of live RAW 264.7 macrophage cells. The cells were incubated with 5 mM **2** for 15 min: (a) bright-field transmission image, (b) blue channel, (c) green channel, and (d) ratio image generated from (c) and (b); the above cells after addition of 40 mM $PdCl_2$ for another 10 min: (e) bright-field transmission image, (f) blue channel, (g) green channel, and (h) ratio image generated from (g) and (f). Incubation was performed at 37 °C under a humidified atmosphere containing 5% CO_2. Scale bar = 20 mm. Reproduced from *Chem. Commun.*, 2011, **47**, 8656–8658 with permission from The Royal Society of Chemistry. Copyright 2011.

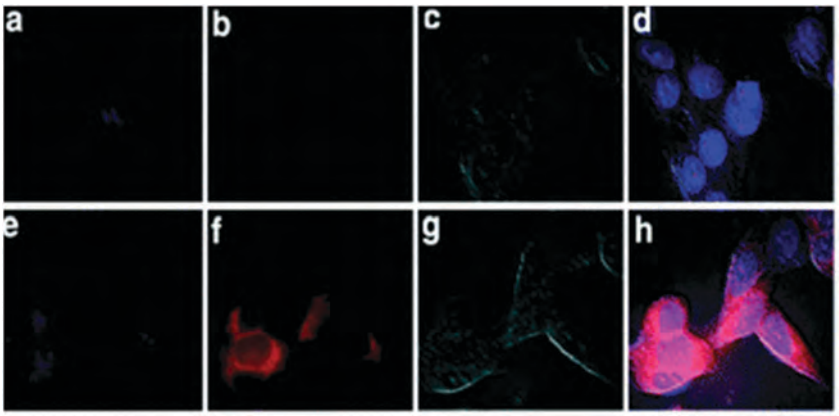

Fig. 4 Fluorescence images of HeLa cells incubated with 50 μM nitrile **4** in the absence (a: blue channel; and b: red channel) and in the presence (e: blue channel; and f: red channel) of 50 μM of $PdCl_2$. Corresponding differential interference contrast (DIC) images (c and g) and merged images (d and h) of the cells are shown. Reproduced from *Dalton Trans.*, 2013, **42**, 12844 with permission of The Royal Society of Chemistry.

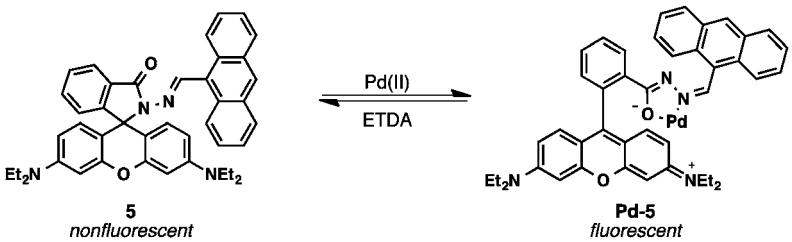

Scheme 4 The spirocycle functionality of **5** quenches fluorescence. Exposure to palladium opens the spirocycle and reinstates fluorescence. Exposure to EDTA sequesters palladium and restores the spirocycle.[68]

In 2013, Zhou, Niu, and coworkers reported a fluorogenic probe for the detection of palladium.[68] Chemosensor **5** forms a fluorescent complex with palladium(II) by opening the spirocycle moiety. Exposure to Pd(II) imparted a purple color and a red fluorescence to the solution, with an emission at 590 nm following excitation at 543 nm. Further investigation indicated a 1 : 1 stoichiometry of Pd(II) to chemosensor **5**. As the fluorescence depended on the opening of the spirocycle, the reversibility of the spirocycle formation was studied. When a mixture of Pd(II) and chemosensor **5** was exposed to EDTA (1 equiv.), the purple color and fluorescence of the solution was lost, indicating that the binding was reversible (Scheme 4).

Chemosensor **5**, possessing favorable amphiphilic properties that facilitate cellular uptake, was employed in Arabidopsis guard cells to image palladium; Arabidopsis guard cells were incubated with 100 μM chemosensor **5** for 40 min in the absence of palladium. Only minimal background fluorescence was observed in the cells. When the cells were treated with 300 μM $PdCl_2$ and subsequently washed after 20 min incubation, a notable increase in intracellular fluorescence was observed (Fig. 5).

In 2014, Kaur and coworkers developed chemosensor **6** for palladium.[69] The aniline unit of **6** quenched the fluorescence of the BODIPY moiety by photoinduced electron transfer (PET). When a metal binds to the sulfur and nitrogen atoms of the dithia-dioxa-aza crown ether (TOAC), PET was inhibited, restoring the fluorescence. To demonstrate reversibility, Na_2S was added to the fluorescent complex **Pd-6**; this procedure

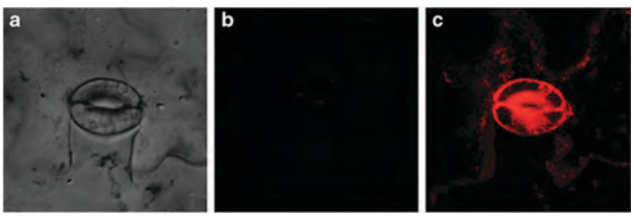

Fig. 5 Confocal fluorescence images of intracellular palladium(II) in Arabidopsis guard cells with **5**. (a) Bright-field transmission image. (b) Confocal fluorescence images stained with 100 μM **5** for 40 min. (c) Confocal fluorescence images stained with 100 μM **5** subsequently exposed to 300 μM $PdCl_2$ for 20 min then rinsed with Tris-HCl buffer three times. The excitation wavelength was 543 nm. Reproduced with permission from *Microchim. Acta*, 2013, **180**, 211–217 with kind permission from Springer Science and Business Media.

successfully restored PET through the sequestering of the palladium (Scheme 5).

As an imaging agent, **6** was tested with MCF-7 cancer cells that were subsequently exposed to Pd(II). The addition of $PdCl_2$ led to an increase in the fluorescence, specifically in the perinuclear region of the cells. No increase in fluorescence was witnessed in the absence of palladium (Fig. 6).

1.3 Imaging palladium in the solid state

Here, we will describe the imaging of palladium in the solid state without sample digestion. Cleaning reactors after

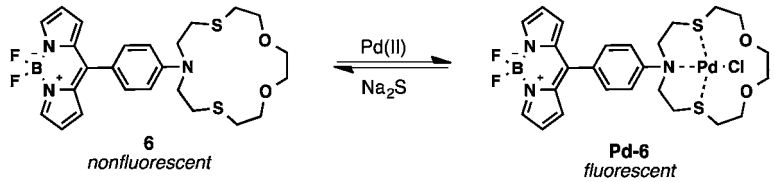

Scheme 5 The fluorescence of the BODIPY moiety in **6** is quenched through photoinduced electron transfer. Exposure to Pd(II) inhibits PET and restores fluorescence. The addition of Na_2S sequesters palladium and reinstates PET.[69]

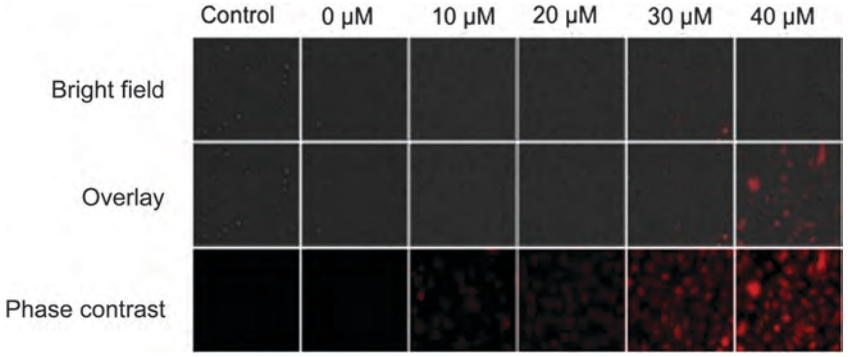

Fig. 6 Confocal images of MCF-7 cells treated with 0–40 μM $PdCl_2$ and 10 μM **6**. Adapted from *RSC Adv.* 2014, **4**, 16104–16108 with permission from The Royal Society of Chemistry. Copyright 2014.

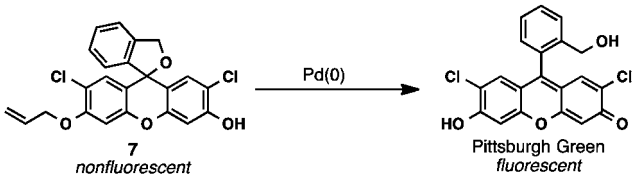

Scheme 6 Exposure of **7** to palladium(0) cleaves the allylic ether bond, releasing Pittsburgh Green. Palladium(0) is formed *in situ* from sodium borohydride reduction of palladium. The reaction also employs tri(2-furyl)-phosphine (TFP) as a phosphine ligand.

palladium-catalyzed reactions is not a trivial task in industry because trace palladium species can cause unintended reactions. As such, it is important, especially in industrial settings, to ensure that the metal is completely removed. To achieve this, Koide coworkers prepared 2′-7′-dichlorofluorescein-based chemodosimeter **7**. Exposure to either Pd(0) or various palladium oxidation states with a reducing agent converted **7** to fluorescent Pittsburgh Green (Scheme 6).[43]

To demonstrate that chemodosimeter **7** can be used for the aforementioned quality control of reactors, used reaction flasks were subjected to **7** to identify palladium-contamination among randomly chosen flasks in the laboratory (Fig. 7a).[70]

Surprisingly, this fluorometric method proved to be quantitative when applied to ore samples without acid digestion, suggesting potential use of the method in the field for imaging palladium in ores without spectrometers (Fig. 7b).[71]

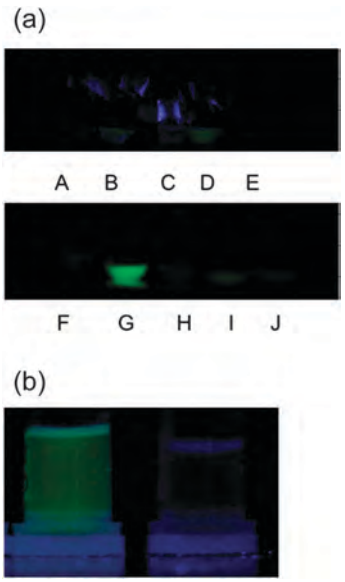

Fig. 7 (a) Photoimages of flasks containing a solution of **7**, $NaBH_4$, and TFP in DMSO/1.23 M phosphate pH 7 buffer (1 : 9, v/v). Flasks E and J were palladium-free controls. The flasks were placed above a UV lamp (325 nm), and the photographs were taken in a dark room. Adapted with permission from John Wiley and Sons; *ChemPlusChem*, 2012, **77**, 281–283. Copyright © 2012 Wiley-VCH Verlag GmbH & Co. KGaA, Weinheim. (b) Left: palladium-containing ore sample with **7**; right: palladium-absent ore sample with **7**. Reprinted with permission from *Ind. Eng. Chem. Res.*, 2013, **52**, 8612–8615. Copyright 2013 American Chemical Society.

1.4 Imaging using palladium microsystems

Beyond imaging of palladium species, the unmasking of fluorescent compounds has been undertaken *in vitro* and *in vivo* through the development of palladium microsystems. Palladium microspheres and resins can be implanted into cellular environments as palladium sources without relying on the uptake of various salts. Once implanted, these microsystems can be used to affect palladium-promoted chemistry.

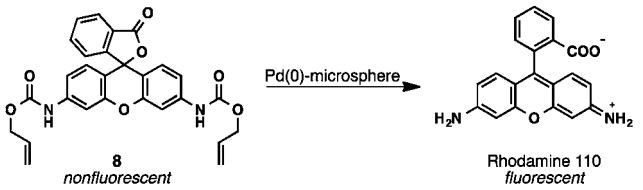

Scheme 7 Exposure of **8** to palladium(0) microspheres cleaves the allylic carbamate bonds and releases fluorescent rhodamine 110.[60]

In 2011, Bradley reported the first Pd(0)-mediated uncaging of a bioactive molecule by means of deallylation in cells.[60] Toward this end, the allylcarbamate rhodamine derivative **8** was prepared. Exposure to palladium(0) cleaved the allylic carbamate bonds, releasing rhodamine 110 (Scheme 7).[60,72]

Fluorescence microscopy revealed that fluorophore-tagged Pd(0) microspheres entered into the cytoplasm of HeLa cells; when HeLa cells were treated with **8**, the cellular uptake was reversible due to its lipophilic nature. When the HeLa cells contained palladium(0) microsphere and were exposed to **8**, the allylcarbamate groups were cleaved, releasing hydrophilic rhodamine 110, which was retained in the cytoplasm (Scheme 7). The imaging of a single fixed HeLa cells revealed that the produced rhodamine 110 is diffused throughout the cytoplasm along with the microspheres (Fig. 8).[60]

In 2014, an *in vitro* method for imaging palladium was demonstrated by Bradley, Unciti-Broceta, and coworkers while developing a bioorthogonal organometallic (BOOM) methodology for the conversion of prodrugs to drugs *via* depropargylation (Scheme 8).[73] The lipophilic nature of nonfluorescent alkyne **9** allowed for facile passage through "biological barriers" in zebrafish, whereas the hydrophilic nature of the unmasked rhodamine enabled retention of the compound. Implanted palladium(0) resins in the yolk sac of the zebrafish cleaved the propargylic carbamate groups of alkyne **9**, releasing the fluorescent rhodamine 110, which was trapped in the yolk sac (Fig. 9).[73]

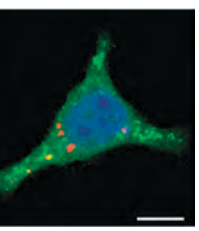

Fig. 8 Merged confocal image of a single HeLa cell fixed with paraformaldehyde, showing nucleus stained with Hoechst 33342 (blue), Texas Red-labeled microspheres (red), and deprotected rhodamine 110 (green). Scale bar is 10 μm. Reprinted with permission from Macmillan Publishers Ltd: *Nat. Chem.*, 2011, **3**, 239–243. Copyright 2011.

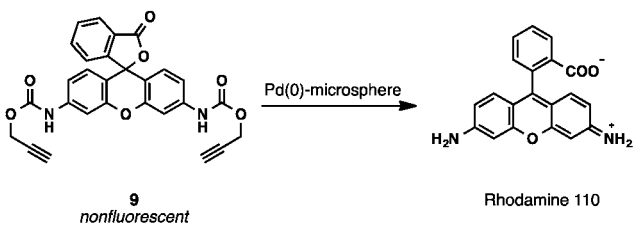

Scheme 8 Synthesis of alkyne **9** from rhodamine 110. Exposure to palladium(0) cleaves the carbamate groups and releases fluorescent rhodamine 110.[73]

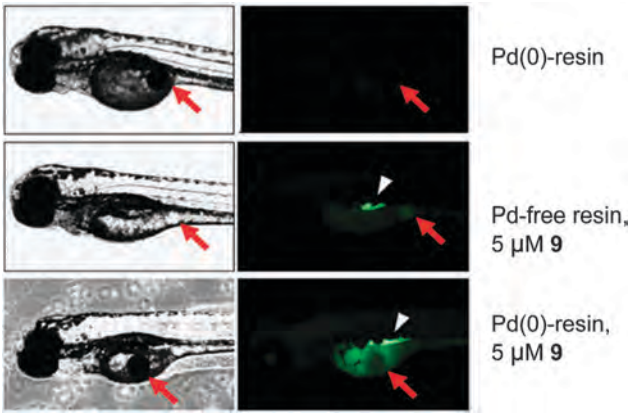

Fig. 9 *In vivo* carbamate cleavage of alkyne **9**. One day after implantation, zebrafish embryos (n = 5) containing a Pd(0)-resin (black color) or a Pd-free resin (white color) in the yolk sac were incubated with alkyne 5 μM **9** for 24 h at 31 °C. Subsequently, zebrafish were imaged using confocal microscopy (Ex/Em: 488/521 nm). Pd(0)-resins and Pd-free resin are indicated with red arrows. Fluorescently labeled gastrointestinal tract is indicated with a white arrow. Reprinted with permission from Macmillan Publishers Ltd: *Nat. Commun.*, 2014, **5**, 3277. Copyright 2014.

The exploitation of facile, reversible uptake of a lipophilic molecule followed by bioorthogonal cleavage to allow for retention of a fluorescent labeling in cellular environments is a novel development for palladium as an imaging reagent. A similar trapping was observed by Koide and coworkers using Pittsburgh Green,[74] supporting the retention of the hydrophilic fluorophore. With these works, manipulation of embedded palladium to unmask fluorescent molecules affords new imaging agents.

1.5 Exploiting palladium-catalyzed carbon–carbon bond forming reactions as an imaging method

Though methods have been developed to directly image palladium or use intracellular palladium to uncage fluorescent molecules, other imaging methods have been developed that harness palladium's cross-coupling potential for protein tagging or formation of fluorescent molecules for localization studies. These methods rely on the uptake of palladium into a cellular environment can be manipulated to afford tagged proteins of interest or fluorophores through formation of new carbon–carbon bonds mediated by palladium.

Bradley reported the use of cytoplasm-localized Pd(0) microspheres as discussed above.[60] Additionally, these microspheres were used in a Pd(0)-catalyzed Suzuki–Miyaura coupling to transform the nonfluorescent aryl triflate **10** into the fluorescent derivative **12** within HeLa cells. Reversible cellular uptake of both triflate **10** and alkylaminophenylboronate derivative **11** facilitated the formation of **12** by the palladium microspheres in the cytoplasm of the cells (Scheme 9). Treatment of the cells with MitoTracker indicated that whereas the fluorescent

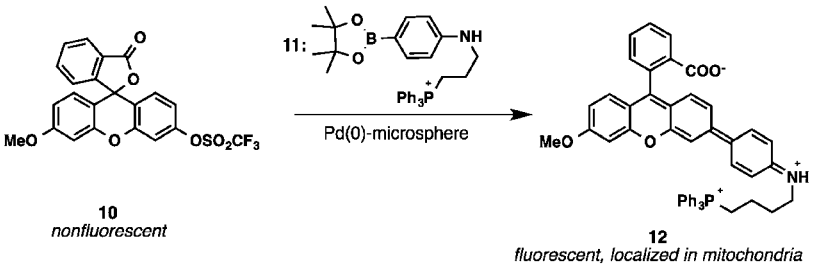

Scheme 9 *In vitro* synthesis of anthofluorescein derivative **12** from **10**, mediated by cytoplasm-localized palladium(0) microspheres. Following formation of the fluorescent product, **12** is directed to the mitochondria by the lipophilic cation.[60,75]

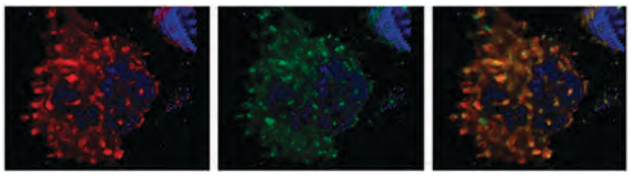

Fig. 10 HeLa cells were loaded with Pd(0)-microspheres, washed to eliminate extracellular palladium(0)-microspheres, and subsequently incubated for 48 h with 20 μM **10** and 20 μM **11**. Mitochondria were stained with MitoTracker Deep Red (red), fixed with paraformaldehyde, and nuclei were stained with Hoechst 33342 (blue). Left panel: cell nucleus (blue) and mitochondria (red). Center panel: cell nucleus (blue) and *in cellulo* synthesized **12** (green). Right panel: merged image (orange indicates co-localization). Reprinted with permission from Macmillan Publishers Ltd: *Nat. Chem.*, 2011, **3**, 239–243. Copyright 2011.

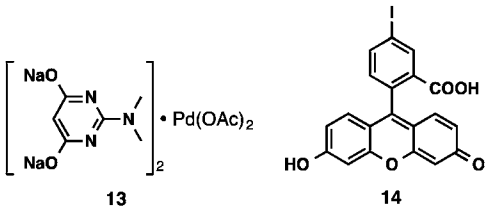

Fig. 11 Palladium complex **13** and fluorescein derivative **14** used by Lin.[62]

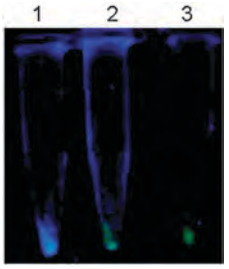

Fig. 12 Fluorescent labeled HPG-Ub by **14** in *E. coli* cells *via* copper-free Sonogashira cross-coupling. Cell pellets shown upon excitation at 365 nm. Pellet 1, cells collected after treatment with 100 μM **14** but not palladium complex **13**; Pellet 2, cells collected after treatment with 100 μM **14**, 1 mM palladium complex **13**, 5 mM sodium ascorbate in Na_2HPO_4 buffer at 37 °C for 4 h; Pellet 3, cells collected after treatment with the preactivated mixture of palladium complex 1 mM **13** and 100 μM **14**. Adapted with permission from *J. Am. Chem. Soc.*, 2011, **133**, 15316–15319. Copyright (2011) American Chemical Society.

product was localized within the mitochondria, the Texas Red-labeled palladium microspheres were not (Fig. 10). The localization is likely due to the lipophilic cation, which directs accumulation in mitochondria.[75]

This work was the first report of a heterogeneous Pd(0) catalyst for labeling intracellular molecules as it can lie dormant after cellular uptake or perform bioorthogonal reactions *in vitro*. This is also the first report of a non-enzymatic aryl–aryl bond formation in living cells. This seminal work has established the groundwork for the conjugation of fluorescent molecules with targeting moieties in live cells to image different cellular components.

In 2011, Lin and coworkers disclosed a palladium-catalyzed bioorthogonal labeling of a genetically encoded alkyne within *E. coli*.[62] Previous attempts at such a labeling were thwarted by the requirement for adding a cytotoxic copper reagent.[63,64] With water-soluble palladium complex **13** (Fig. 11), Sonogashira coupling between fluorescein iodide **14** and an alkyne-incorporated protein selectively labeled a homopropargylglycine-tagged ubiquitin (HPG-Ub), encoded from genetic code expansion, within bacteria without adding copper. In the absence of the palladium-complex, no tagging was observed. The addition of palladium complex **13**, fluorescein iodide **14**, and sodium ascorbate to M15A cells overexpressing HPG-Ub led to fluorescence enhancement within the cells compared to a palladium-free control (Fig. 12).[62] This imaging method utilizing palladium is remarkable, as it allowed for the tagging of a terminal alkyne in a protein of interest under non-cytotoxic conditions.

In 2012, Davis and coworkers disclosed palladium-mediated cell surface labeling in *E. coli*.[76] To study the OmpC protein homotrimer, they identified "tag" sites to incorporate an unnatural amino acid, *p*-iodophenylalanine (*p*IPhe), and employed **15** (Fig. 13) as a palladium species to affect the coupling of the screened combinations of OmpC mutants (N47X, N188X, Y232X, Y310X), OmpC-Y232X showed the most effective tagging with boronic acid **16**, in which X refers to the *p*IPhe incorporation (Fig. 14). Control experiments revealed that not only is this location the most accessible of the tested "tag" sites, but the reaction is not affected by the addition of reducing sugars, such as D-glucose.[76]

The palladium concentration-dependence for the labeling indicated an upper threshold of 0.45 mM, above which no additional labeling occurred. At this threshold value, cell death was observed at <3%. Higher concentrations revealed that concentrations as high as 1.9 mM **15** led to only 36% observed cell death in induced cells of the JW2203-1 cell line.[76] This is

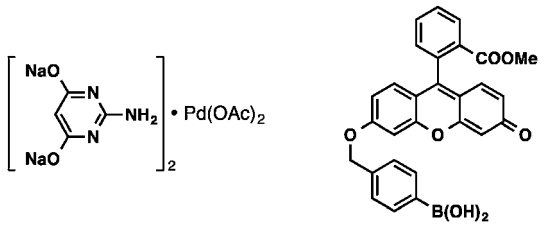

15 16

Fig. 13 Palladium complex **15** and boronic acid **16** used by Davis.[76]

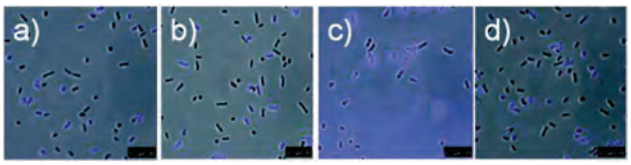

Fig. 14 Labeling of OmpC mutants: (a) N47X, (b) N188X, (c) Y232X, (d) Y310X with 1.6 mM **16** and 0.35 mM **15** for 1 h at 37 °C in a pH 8 phosphate buffer. Scale bar: 100 μm. Reprinted with permission from *J. Am. Chem. Soc.*, 2012, **134**, 800–803. Copyright (2012) American Chemical Society.

noteworthy because it indicates potential for palladium-mediated labeling and carbon–carbon bond formation at non-toxic levels of palladium reagents.

In 2013, Chen reported an improvement on the use of *in cellulo* palladium-catalyzed Sonogashira coupling for imaging protein.[61] Preparation of unnatural amino acid **17** (Fig. 15), followed by incorporation into green fluorescent protein (GFP) bearing an amber codon at Asp149 afforded the GFP–**17** conjugate; this protein was used for imaging due to inherent fluorescence that could be further increased upon conjugation with fluorescent compound **17** (Fig. 15).[61]

Screening various palladium reagents to effect the coupling of the alkyne moiety of GFP–**17** and iodide **18** afforded the highest catalytic activity with Na_2PdCl_4 and $Pd(NO_3)_2$. The addition of a water-soluble ligand (2-amino-4,6-dihydroxypyrimidine disodium salt, 2-(dimethylamino)-4,6-dihydroxypyrimidine disodium salt, N^2,N^2-dimethylpyrimidine-2,4,6-triamine) proved detrimental to the reaction efficiency. Using a biotinylated derivative of **18**, they discovered that the $Pd(NO_3)_2$ did not negatively impact the native protein folding within the time measured for labeling (0–60 min).[61]

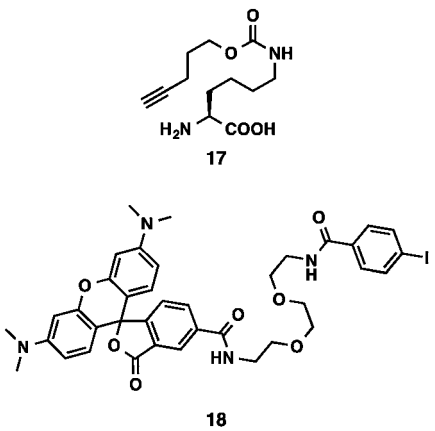

17

18

Fig. 15 Propargylated unnatural amino acid **17** and aryl iodide **18** used by Chen.[61]

The palladium and aryl iodide concentrations were optimized using *E. coli* cells expressing the GFP–**17** protein conjugate. These bacteria were incubated with various concentrations of iodide **18** and $Pd(NO_3)_2$. The washed cells were lysed and analyzed by SDS-PAGE. 200 μM $Pd(NO_3)_2$ and **18** proved to be the optimal concentration for labeling for each reagent respectively. Studies in *E. coli* also confirmed specificity for this labeling using an azido-pyrrolysine analogue as a control. At these concentrations, $Pd(NO_3)_2$ was found to be relatively non-toxic; no membrane damage occurred after exposure to 200 μM $Pd(NO_3)_2$ for 1 h. For further imaging, alkyne **17** was incorporated into the OspF residue at K102 inside *Shigella*. *Shigella* was exposed to 200 μM iodide **18** and 200 μM $Pd(NO_3)_2$ (Fig. 16). Analysis by SDS-PAGE revealed a single band corresponding to the labeled protein, indicating the utility of this imaging method within Gram-negative bacteria.[61]

In 2014, Chen and coworkers reported the use of water-soluble N-heterocyclic carbene (NHC)-stabilized palladium complexes for bioorthogonal labeling of proteins on the surface of mammalian cells.[77] Identification of catalytically active Pd–NHC complex **19** (Fig. 17) facilitated Suzuki–Miyaura coupling on the surface of tagged live mammalian cell surfaces. Free lysine residues on the protein surface were activated with **20**, followed by **19**-mediated Suzuki–Miyaura coupling (Fig. 17).[77]

Mammalian cell membranes were activated with 60 μM **20** followed by exposure to 80 μM **19** and 200 μM **21**. In the

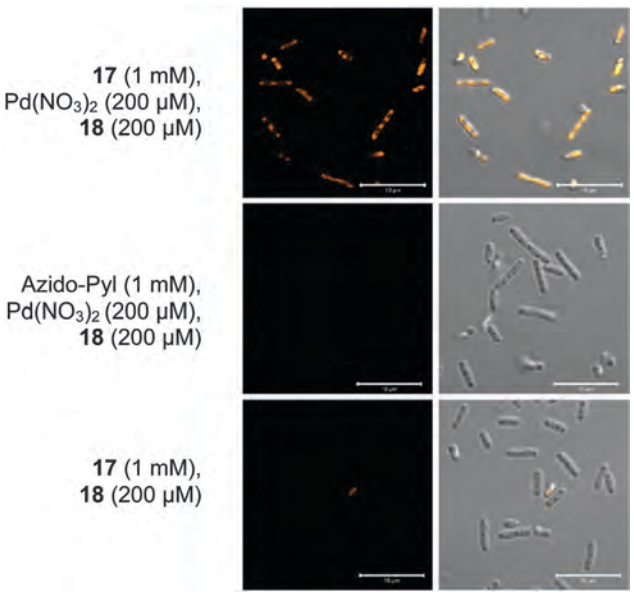

Fig. 16 Confocal microscopic imaging of $Pd(NO_3)_2$-triggered Sonogashira coupling for site-specific labeling of OspF-K102-**17** protein inside *Shigella* with 200 μM $Pd(NO_3)_2$ and 200 μM **18**. Azido-pyl (azido-pyrrolysine) was the vector for incorporation of **17**. As a control, it was used without unnatural amino acid supplementation. Scale bar: 10 μm. Adapted with permission from *J. Am. Chem. Soc.*, 2013, **135**, 7330–7338. Copyright (2013) American Chemical Society.

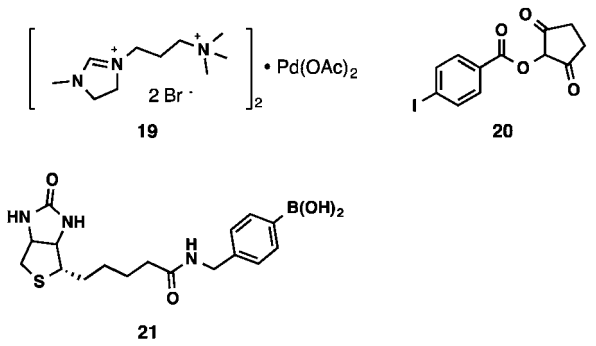

Fig. 17 Palladium–NHC complex **19**, protein surface preactivation reagent **20**, and biotinylation reagent **21** used by Chen.[77]

absence of the **19** or the preactivation with **20**, there was no observed labeling (Fig. 18).[77]

Additionally, using HeLa and A549 cell lines, catalyst **19** was found to be relatively nontoxic (>85% viability) for concentrations 2.5 times higher than those used in the cell labeling.[77] This work emphasizes the utility of a palladium-catalyzed bioorthogonal method for imaging, using a preactivation of the cell surface, instead of incorporation of an unnatural amino acid; without requiring genetic code expansion, free lysine residues can be activated toward tagging, facilitating easier tagging for proteins of interest.

In 2012, Chang and coworkers used palladium as part of an imaging-enabling agent for carbon monoxide, a second messenger, using a palladium-catalyzed carbonylation for carbon monoxide detection.[78] Using a BODIPY core, the fluorescence of **22** was quenched by palladium as a heavy-atom effector. This dimeric species acted as an activated precursor to react with carbon monoxide to form the fluorescent compound **23** (Scheme 10).[78]

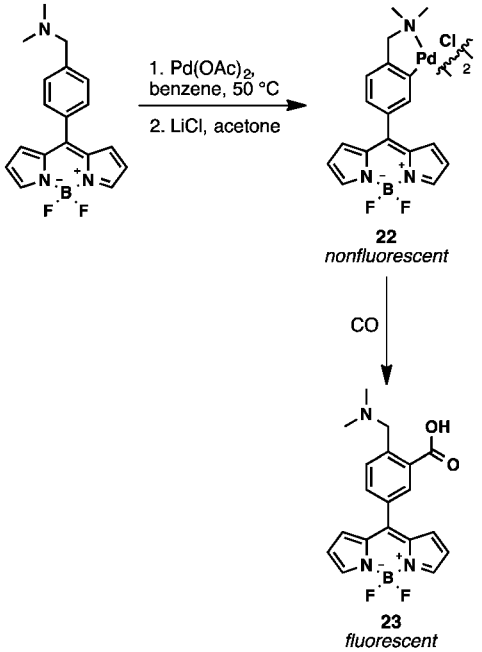

Scheme 10 Conversion of nonfluorescent **22** to fluorescent **23** upon exposure to carbon monoxide.[78]

When tested against other second messengers (H_2O_2, *t*BuOOH, NaOCl, $O_2^{\bullet -}$, NO, $ONOO^-$, and H_2S), the probe was found to be selective for carbon monoxide with only a small responsiveness to H_2S.[78] Incubation of HEK293T cells with 5 or 50 μM [$Ru(CO)_3Cl$(glycinate)], a molecule that releases carbon monoxide, followed by 1 μM **22** led to an increase in intracellular fluorescence in a dose-dependent manner with respect to CO (Fig. 19). Two separate assays confirmed the nontoxic nature of the probe itself.[78]

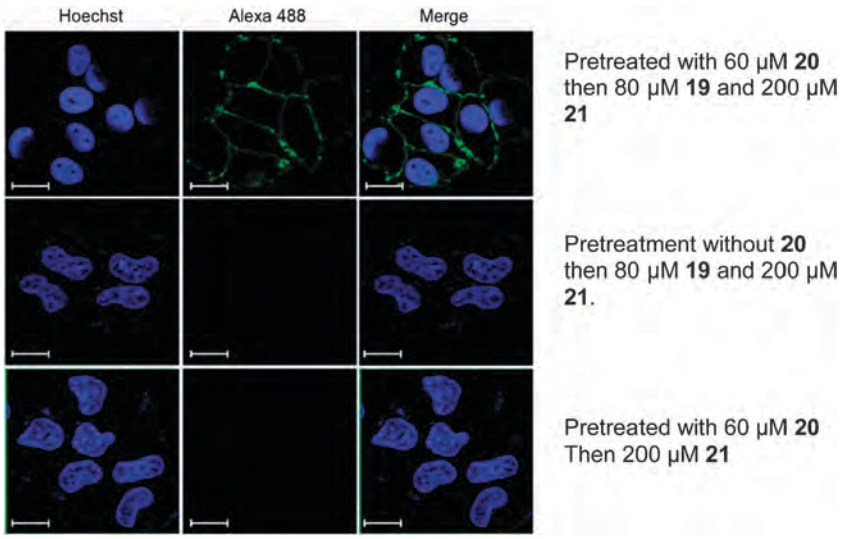

Fig. 18 Pd-mediated cross coupling of membrane proteins on the mammalian cell surfaces. Fluorescence microscopy images of living HeLa cells following pretreatment with 60 μM **20** followed by 80 μM **19** and 200 μM **21** for 1 h in a pH 8 phosphate buffer (top). As negative controls, a labeling reaction was performed with cells not pretreated with **20** (central) or in the absence of **19** (bottom). Scale bar: 10 μm. Streptavidin conjugated to Alexa 488 was used to tag biotinylated cell surfaces. Adapted with permission from *J. Org. Chem.*, 2014, **79**, 8652–8658. Copyright (2014) American Chemical Society.

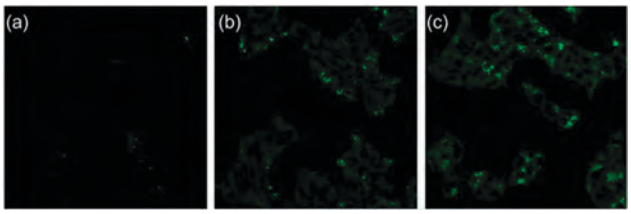

Fig. 19 Confocal microscopy images of CO detection in live HEK293T cells using **22**. (a) HEK293T cells incubated with 1 μM **22** for 30 min at 37 °C. (b) HEK293T cells incubated with 5 μM [$Ru(CO)_3Cl$(glycinate)] for 45 min at 37 °C and 1 μM **22** for the final 30 min. (c) HEK293T cells incubated with 50 μM [$Ru(CO)_3Cl$(glycinate)] for 45 min at 37 °C and 1 μM **22** for the final 30 min. Adapted with permission from *J. Am. Chem. Soc.*, 2012, **134**, 15668–15671. Copyright (2012) American Chemical Society.

Similar to previous imaging methodologies, this indicates the potential for palladium as an imaging-enabling reagent, facilitating the formation of carbon–carbon bonds in live cells without severe toxicities. This work highlights the potential for palladium to mediate detection of second messengers and other small molecules in cells.

1.6 Near-infrared probes for palladium detection *in vivo*

With previously outlined fluorogenic probes, there are drawbacks regarding the excitation and emission wavelengths, limiting utility in *in vivo* applications. Light from the near-infrared (NIR) region has better tissue permeation with less tissue damage and is therefore more desirable for *in vivo* applications.[79] Despite this, palladium-imaging methods for bio-imaging are scarce.

In 2013, Lin and coworkers disclosed an NIR fluorescent "turn-on" and ratiometric probe for imaging palladium based on the cleavage of an aryl propargylic ether bond.[80] Conjugation of a propargylic ether to the phenolic group of an NIR dye, fluorescence was quenched. Exposure to $PdCl_2$ cleaved the ether and unmasked fluorescence at 716 nm, demonstrating up to a 43-fold enhancement upon excitation at 690 nm (Scheme 11). Additionally, comparison of the fluorescence intensities at 716 and 760 nm following excitation at 645 nm allowed for use of **24** as a ratiometric probe.[80]

As an imaging agent, 5 μM propargylic ether **24** was loaded into HeLa cells, which were subsequently exposed to 50 μM $PdCl_2$. In the absence of $PdCl_2$, the cells were nonfluorescent, but cells containing $PdCl_2$ were fluorescent. Nuclear staining with Hoechst 33258 showed that **25** was localized in the cytoplasm of the cells. Subsequent MTT assay indicated that 10 μM **24** was not cytotoxic.[80] As such, **24** proved useful as an NIR probe for imaging palladium (Fig. 20).

In 2014, Guo, Zhu, and coworkers developed an NIR ratiometric method for imaging intracellular palladium based on Tsuji–Trost allylic cleavage.[81] Exposure of allyl carbonate **26** to Pd(0) cleaves the allylic carbamate, recovering the conjugation of the π-electrons in the cyanine dyes (Scheme 12). The emission corresponding to **26** upon excitation at 740 nm at 825 nm is lost upon this cleavage and a new band corresponding to ketone **27** was seen upon excitation at 545 nm with an emission at 655 nm (Scheme 12). This concomitant shift allows for the use of **26** as a ratiometric probe for imaging palladium in living cells, although it is not clear what types of palladium reagents were used in these experiments or at what concentrations. Allyl carbonate **26** was also used for colorimetric palladium imaging on paper strips.[81]

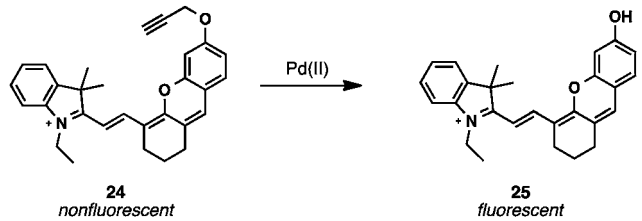

Scheme 11 Exposure of **24** to Pd(II) cleaves the propargylic ether and unmasks fluorescence at 716 nm following excitation at 690 nm.[80]

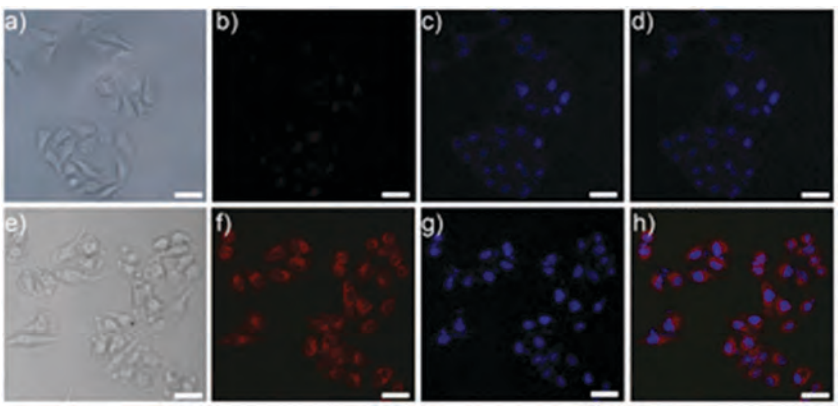

Fig. 20 Brightfield and fluorescence images of HeLa cells with the probe **24**: (a–d) bright-field and fluorescence images of the cells only incubated with 5 μM **24** and 4.5 μM Hoechst 33258 for 30 min: (a) bright-field image; (b) fluorescence image from the red channel; (c) fluorescence image from the blue channel (nuclear staining), and (d) overlay of (b) and (c); (e–h) bright-field and fluorescence images of the cells incubated with 5 μM **24** and 4.5 μM Hoechst 33258 for 30 min, and then addition of 50 μM $PdCl_2$ for another 30 min: (e) bright-field image; (f) fluorescence image from the red channel, (g) fluorescence image from the blue channel (nuclear staining), and (h) overlay of (f) and (g). Scale bar: 40 μm. Reproduced from *Org. Biomol. Chem.*, 2013, **11**, 1938–1941 with permission of The Royal Society of Chemistry.

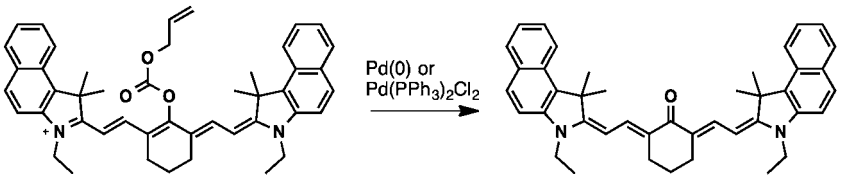

26
Ex 740 nm Em 825 nm

27
Ex 545 nm Em 655 nm

Scheme 12 Exposure of allyl carbonate **26** to Pd(0) restores conjugation between the NIR moieties and shifts maximum fluorescence from 825 nm (ex. 740 nm) to 655 nm (ex. 545 nm). Phosphine-bound Pd(II) species also catalyzed the reaction.

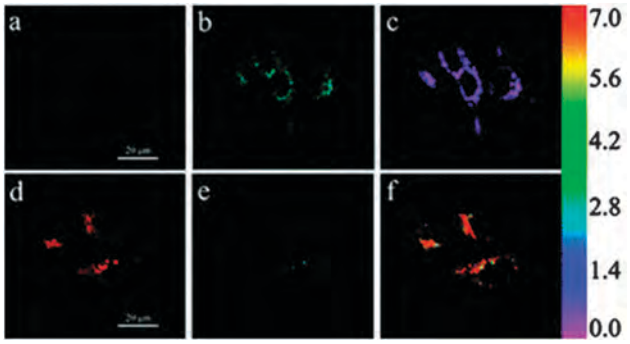

Fig. 21 Confocal fluorescence images of HeLa cells incubated with **26** (a) and (b) for 25 min; then treated with palladium for 25 min (d) and (e). (a) and (d) λ_{ex} = 540 nm, collected in optical windows between at 600–700 nm (red channel); (b) and (e) λ_{ex} = 633 nm, collected in optical windows between at 700–750 nm (cyan channel); (c) and (f) pseudocolored ratiometric ratio was collected in two channels (F_{red}/F_{cyan}). Note: the ratiometric images were obtained by the image analysis software, Image Pro-plus 6.0 (scale bar = 20 μM). Reproduced from *Chem. Commun.*, 2014, **50**, 13525–13528 with permission of The Royal Society of Chemistry.

In vivo applications were tested using HeLa cells incubated with 10 μM **26** which were subsequently exposed to palladium of an unknown oxidation state and concentration. Prior to the exposure to palladium, a notable NIR signal was found, indicating cell permeability. Following exposure to palladium, notable changes in the red channel for fluorescence were observed (Fig. 21). The fluorescence intensities could be correlated, showcasing the use of **26** as a ratiometric imaging method for palladium in live cells.[81]

1.7 Conclusions

Collectively, these examples indicate the viability of using palladium as a tool for imaging. Imaging of intracellular palladium through exposure to palladium-responsive fluorogenic molecules has demonstrated utility through use of palladium microspheres and resins as well as palladium salts. Rapid and reversible uptake of a lipophilic starting material facilitates passage into cellular environments followed by retention of the hydrophobic product upon exposure to palladium.

Through the recent surge of BOOM chemistry, palladium as part of an imaging tool to tag proteins of interest and organelles stands to gain confidence. Additionally, palladium being harnessed to detect transient biological species is a developing field, allowing for facile detection of previously undetectable species in living systems. As palladium is being used more frequently in BOOM chemistry, it may become essential to ensure the presence of palladium.

2. Platinum imaging methods

2.1 Introduction

Platinum is highly relevant in clinical oncology, as platinum-based drugs are staples in cancer therapy today,[82–90] and yet no truly platinum-selective chemodosimeters have been reported. Further, presumably because of similar reactivity between palladium and platinum, none of the developed chemodosimeters are selective for platinum over palladium. Although cisplatin has been used as a chemotherapeutic agent for decades, much is still unknown about its mechanism of action, including intracellular localization. Even though its ability to form adducts with purines has been attributed to its cytotoxic properties, a fully comprehensive understanding of its distribution and targets within the cell has yet to be realized; for example, just recently, it was shown that binding to tRNA may be a cause of cytotoxicity.[91] The lack of platinum-specific imaging methods has impeded the ability to accurately apply chemotherapy regimes and to develop new platinum-based drugs.

To prevent cisplatin-associated toxicities in the clinic, dosing methods according to body surface area measurements are applied. However, the models developed to apply chemotherapy regimes may underdose or overdose patients.[92–114] Appropriate chemotherapy regimes are critical when treating patients with poor prognoses or compounding factors. The development of a fluorometric method of cisplatin quantification is needed to more effectively apply chemotherapy. For use in this setting, these fluorometric methods must be able to quantify 0.2 to 11 μM cisplatin in serum.[99–101] Further, they must be rapid enough to obtain measurements at least every 4 h to be applied to the case of cisplatin overdose.[101,115]

Despite the lack of platinum-specific imaging methods, platinum-based anticancer drugs continue to be developed; for example, polymer-bound cisplatin was found to be effective against solid tumors in mice.[116] In this study, platinum concentrations were measured in 208 plasma samples by atomic absorption spectroscopy.[116] Pharmacokinetic studies of this breadth would be more facile and affordable if a high throughput method were available for quantifying platinum.

2.2 Chemosensors for platinum

The first platinum detection method was reported in 1951. *p*-Nitrosodiphenylamine (Fig. 22) showed coloration in the

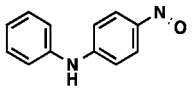

Fig. 22 The structure of *p*-nitrosodiphenylamine used by Ryan to detect several cations.

presence of platinum group metals. Boiling platinum(IV) chloride with *p*-nitrosodiphenylamine resulted in the formation of an intense red color after 10 min with a limit of detection of approximately 5 μM. However, this method suffered from significant interference from palladium, rhodium, gold, and iron and is highly dependent on salt concentrations and pH.[117]

The first fluorometric method for platinum was reported by Garner and Koide, in which the combination of platinum and Ph_3P catalyzed the conversion of chemodosimeter 7 (Fig. 23a) to Pittsburgh Green. This method allowed for detection of platinum ions even at 100 nM, but remained more responsive to palladium.[37] This is also the first quantitative fluorometric method for platinum concentrations in complex samples. The dynamic linear range was observed roughly in the 0–526 nM range.[118] As expected for catalytic systems, the fluorescence signals continued to increase linearly over time, indicating that lower concentrations of platinum ions may be quantified if the assay is performed for a longer time. This method was used by Park, Kim, and coworkers to quantify platinum ions in complex samples.[119] Attempts to develop more platinum-selective method using 7 at various pHs were unsuccessful, only resulting in more palladium-selective method at pH 4.[37] The roles of Ph_3P have not yet been elucidated in detail.

In 2010, the Tae group developed a rhodamine triazole-based chemosensor for Pt^{2+} (Fig. 23b). The reversible binding between Pt^{2+} and probe **28** occurred under aqueous conditions. The putative platinum-probe complex **Pt-28** was proposed by the authors. Prior to addition of Pt^{2+}, the solution of **28** shows neither color nor fluorescence, suggesting that it exists predominately in the spirocyclic form. Binding occurs in a 1 : 1 fashion and allows for detection at 125 nM. The standard deviation values were not reported; thus, a more statistically robust limit of detection remains to be seen. Not surprisingly, Pd^{2+} was able to induce a slight fluorescence signal. Additionally, Pd^{2+} significantly altered the color of the solution. This sensor was applied to cisplatin detection; although detection was possible in water, cisplatin showed a smaller fluorescence signal compared with those obtained with platinum salts. This method was not applied to any complex samples other than pure water.[120]

The Ang group reported a rhodamine-based probe conjugated to diethyldithiocarbamate for Pt(II) recognition (Fig. 23c; **29**). They envisioned that platinum would bind through the dithiocarbonyl bond, allowing opening of the spirolactam ring and turning on fluorescence. The probe observed a 65-fold increase in fluorescence within 5 min upon addition of K_2PtCl_4. Detection of cisplatin required 1 h; it is unclear how the fluorescence intensity upon addition of cisplatin compared to that of K_2PtCl_4. They postulated, on the basis of mass spectroscopy, that the platinum–Rho–DDTC complex may be compound **Pt-29**. X-ray crystallography was not reported. This method was successfully applied towards imaging 30 μM cisplatin in HeLa cells, although the probe was not able to enter the nuclear compartment

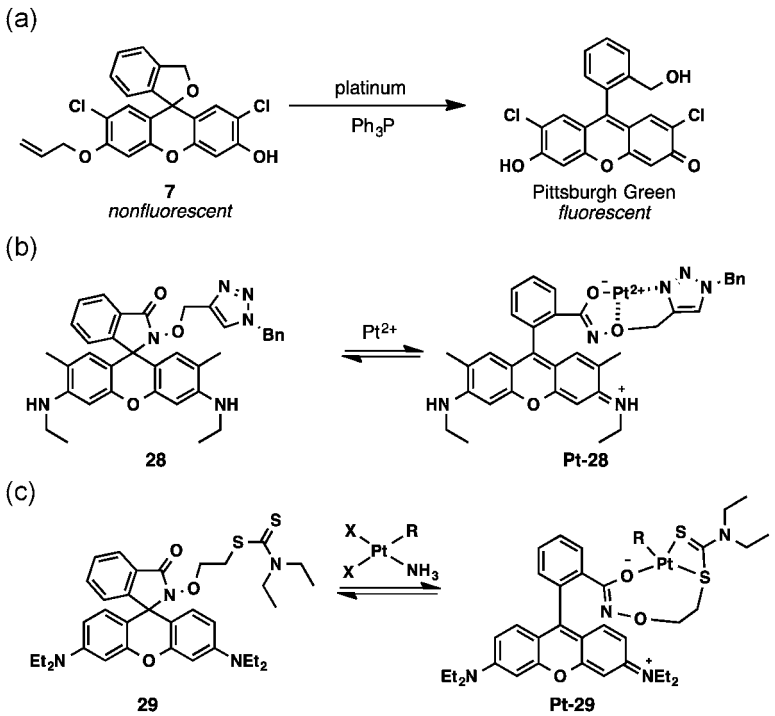

Fig. 23 Structure of chemosensor and fluorescent product developed by (a) Garner and Koide, (b) Tae and coworkers, and (c) Ang and coworkers.

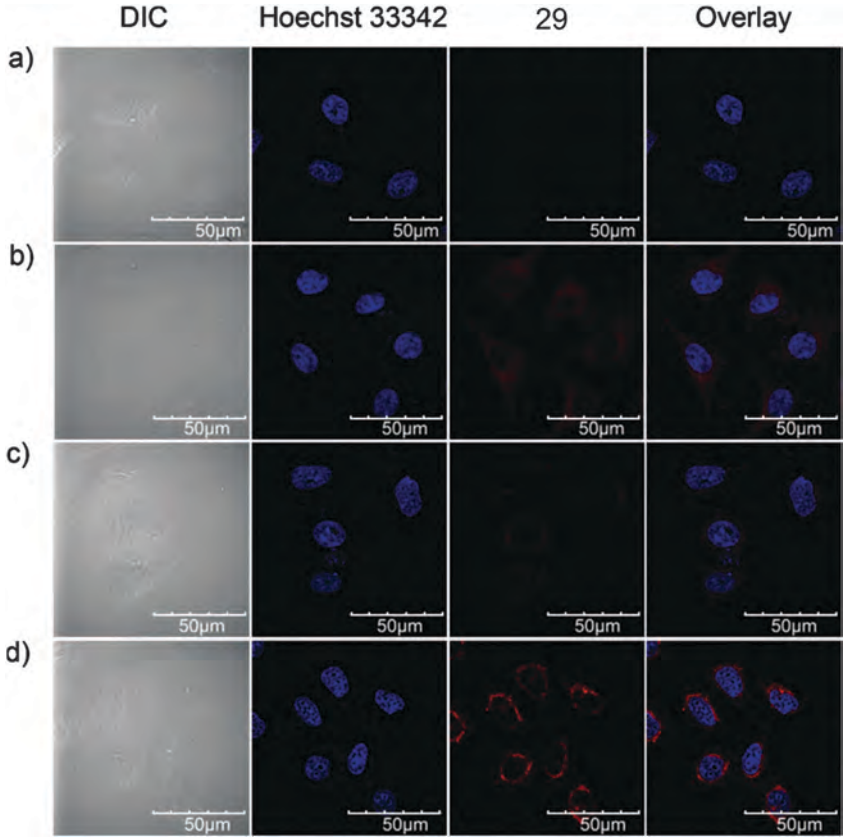

Fig. 24 Merged fluorescence images of HeLa cells. (a) Untreated (control), and exposed to (b) cisplatin, (c) **30**, and (d) **31** (30 μM) for 3 h and further incubated with 30 μM triazole **29** for 1 h at 37 °C. Adapted with permission from John Wiley and Sons, *Angew. Chem.*, 2013, **125**, 12001–12005. Copyright © 2013 Wiley-VCH Verlag GmbH & Co. KGaA, Weinheim.

(Fig. 24); this was sensitive to the platinum species that complexed with triazole **29**.[121] No red fluorescence was observed without the presence of platinum drug (Fig. 24a). Only very slight fluorescence was observed with the complexation of triazole **29** and cisplatin in cells (Fig. 24b); complexation of triazole **29** and platinum compound **30** (Fig. 25) in cells showed similar fluorescence intensities (Fig. 24c). A more intense fluorescence (Fig. 24d) was observed when triazole **29** was incubated with the *O*-benzoyl platinum compound **31** (Fig. 25). The metal selectivity of this method was shown with only a limited set of endogenous metals (Na, K, Mg, Fe(II), Fe(III), Zn(II), and Cu(II)).[121] Although other heavy metals are irrelevant to the intracellular biology of cisplatin, it would be interesting to test this system with other metals such as Pd(II) and Hg(II).

The Bai group developed several conjugated polymer-based sensors (**32–34**; Fig. 26) in 2012. These sensors were used as an on–off switch for Pt detection *via* aggregation-induced

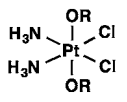

30: R = H
31: R = COPh

Fig. 25 Platinum compounds used by Ang.

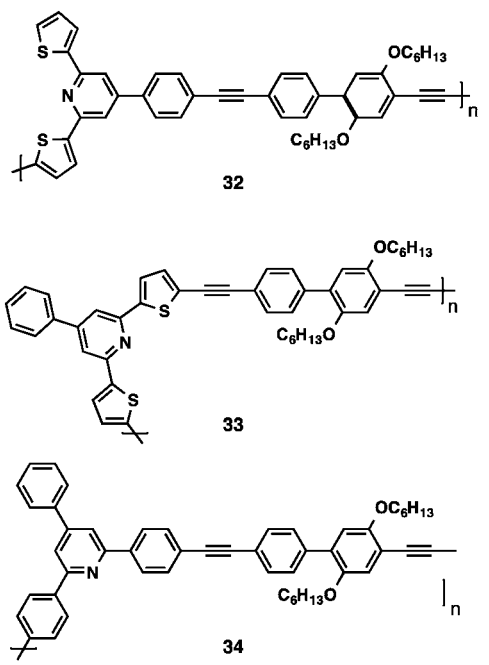

Fig. 26 Polymeric sensors developed by the Bai group.

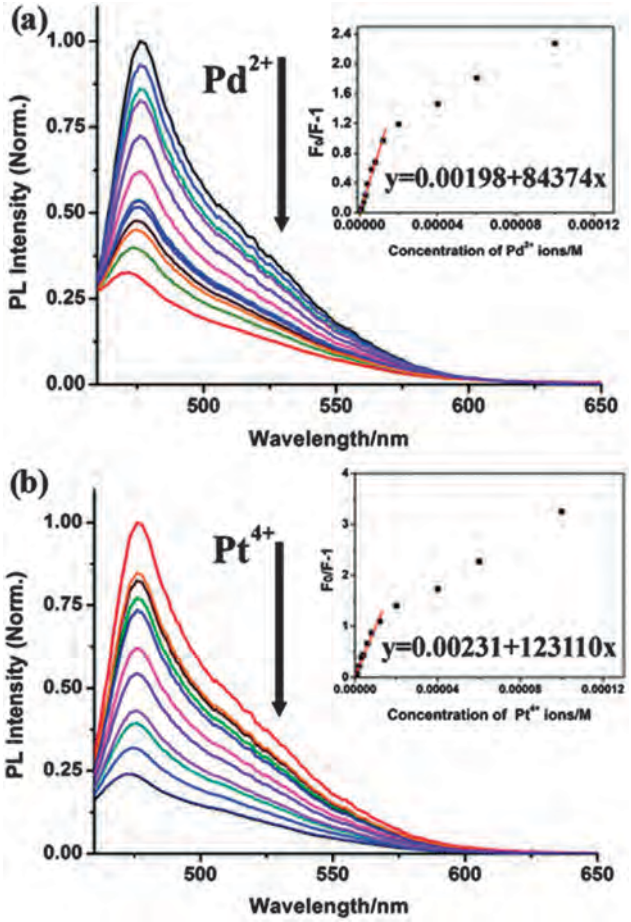

Fig. 27 Fluorescent emission spectra of **32** in the presence of different concentrations (0–10^{-4} M) of (a) Pd^{2+} ions and (b) Pt^{4+} ions in THF : H_2O (1 : 1, v/v) solution with 10 mM HEPES buffer. Inset: fluorescence quenching of **32** by various concentration of (a) Pd^{2+} ions and (b) Pt^{4+} ions, in which F_0 and F denote the intensity of the fluorescence signal of the sensing materials in the absence and presence of the metal ions, respectively. Adapted from *J. Mater. Chem.*, 2012, **22**, 3555–3561 with permission of The Royal Society of Chemistry.

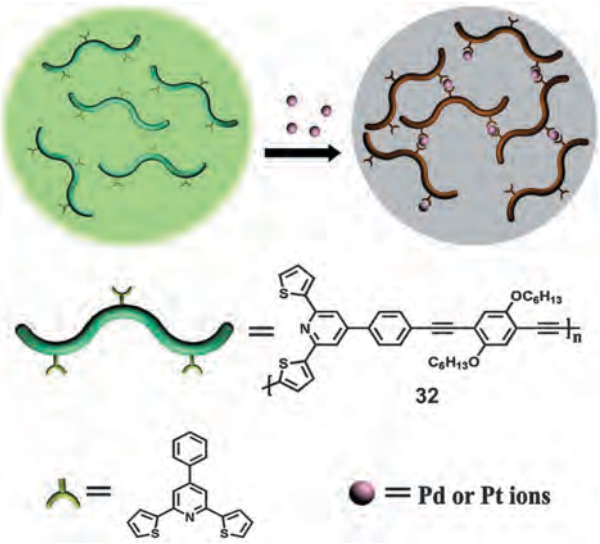

Fig. 28 Schematic illustration of sensing mechanism of **32**. Adapted from *J. Mater. Chem.*, 2012, **22**, 3555–3561 with permission of The Royal Society of Chemistry.

fluorescence quenching and showed decreasing fluorescence in the presence of both Pt (Fig. 27a) and Pd (Fig. 27b). The mechanism of aggregation was postulated in Fig. 28, in which 2,6-dithienyl-4-phenylpyridine as part of the polymer binds to either platinum or palladium ions, causing assembly of polymers. These sensors were equally responsive to both Pt(IV) and Pd(II) and had a limit of detection of 1 μM. Further, this method was very sensitive towards solvent effects.[48]

In sum, truly selective fluorometric methods for submicromolar platinum ions have not yet been developed. Perhaps because of this lack of viable imaging methods for platinum, several studies have attempted to conjugate fluorophores directly to cisplatin or its derivatives in order to monitor the accumulation and distribution throughout the cell.

2.3 Bioimaging of fluorophore-tagged Pt-drugs

2.3.1 Fluorophore-tagged cisplatin and carboplatin analogs. An alternative strategy to monitor the accumulation and distribution of platinum in living cells is to tag the platinum compound itself to a fluorescent molecule. This strategy has been used to study the uptake and intracellular distribution of several platinum drugs.

The Reedijk group attempted to probe the intracellular processing of cisplatin with the use of a cisplatin derivative.[122] Conjugation to 5-(and 6-)carboxyfluorescein diacetate generated the nonfluorescent cisplatin analog **35** (Fig. 29), which is membrane-permeable because the fluorescein is in the neutral form. The esters were hydrolyzed by intracellular esterases to form the fluorescent and membrane-nonpermeable carboxylate **36**. The platinum-free fluorescein diacetate **37**, which was hydrolyzed by the intracellular esterases to form carboxylate **38**, was used to verify that fluorescence distribution in cells was attributed to platinum and not the fluorophore.[122]

The localization within U2-OS cells was monitored by fluorescence microscopy with cisplatin analog **35** and its platinum-free analog **37**. Both compounds were taken into cells within 1–2 h; the localization of cisplatin analog **35** is shown in Fig. 30. After 15 min, this cisplatin analog appeared diffuse throughout the cell (Fig. 30A–C); nuclear accumulation was observed after 2 h (Fig. 30D–F) and distinct speckles in the cytoplasm were observed after 24 h (Fig. 30G–I). The authors claimed that only cisplatin analog **35** was able to accumulate in the nucleus, likely due to the platinum center, and appeared to localize to the Golgi. Further, the same group found that the treatment of a cisplatin-resistant U2-OS cell line with cisplatin analog **35** and the platinum-free analog **37** manifested no differences in uptake, accumulation, or distribution, suggesting that there are no differences in the cisplatin processing systems of resistant cell lines *versus* those that retain sensitivity.[122]

Howell and coworkers utilized the probe developed by the Reedjik group to analyze the intracellular distribution and trafficking of cisplatin within the 2008 (ovarian carcinoma) cell

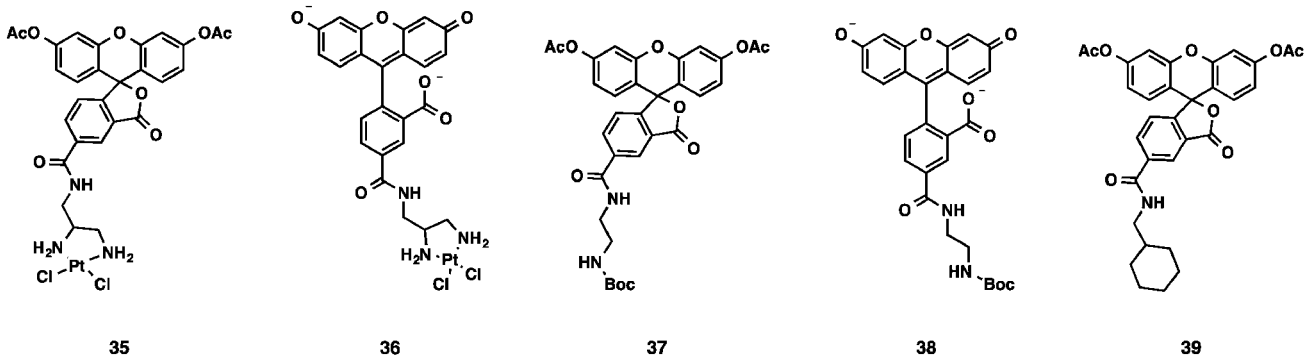

35 36 37 38 39

Fig. 29 Compounds developed by Reedijk and coworkers (**35–38**) and by Hambley and coworkers (**39**). Boc = *tert*-butoxycarbonyl, Ac = acetyl.

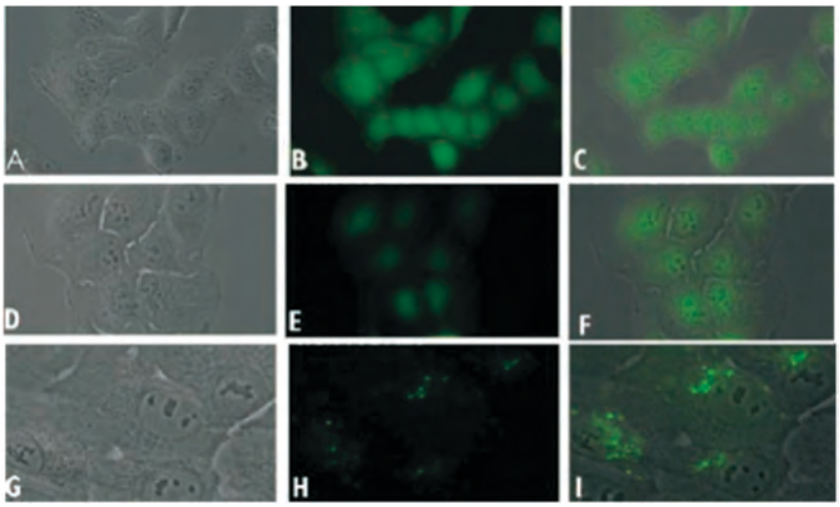

Fig. 30 Cisplatin analog **35** localization in living U2-OS cells. U2-OS cells were incubated for 30 min with 10 μM cisplatin analog **35**. After drug treatment, cells were monitored live using digital inverted microscopy. A–I represents three different time points after incubation, respectively 15 min, 2 h, and 24 h, representative for the observations that were done. For every time point a phase contrast image (A, D, G), the corresponding fluorescence image (B, E, H), and a superimposition (C, F, I) is shown. Cisplatin analog **35** is readily taken up by the cells. After 15 min incubation (A–C), a fluorescent signal is visible throughout the whole cell. After 2 h, a more pronounced nuclear accumulation of cisplatin analog **35** is observed (D–F). After 24 h incubation (G–I), an accumulation in a distinct area in the cytoplasm is visible. The superimposition (I) of the phase contrast image and the fluorescence image shows the intracellular localization of cisplatin analog **35** in living cells. This area in the cell most likely corresponds to the Golgi apparatus. Adapted from *JBIC, J. Biol. Inorg. Chem.*, 2005, **9**, 403–413 with kind permission from Springer Science and Business Media.

line and its cisplatin-resistant counterpart, 2008/C13*5.25.[123] They synthesized the cyclohexyl analog **39** (Fig. 29) to verify that the intracellular distribution of cisplatin analog **35** was due to the platinum center and not the fluorophore. Cisplatin analog **35** showed similar cytotoxicity as cisplatin, with the ratio of the IC_{50} values in resistant and sensitive lines being 5.7 μM for cisplatin and 5.3 μM for cisplatin analog **35**. Analysis of the distribution of the two compounds throughout the cell revealed that the cyclohexyl analog **39** was found mainly in filamentous actin in both the cisplatin-sensitive and cisplatin-resistant cell lines. Cisplatin analog **35** could be found in discrete vesicular compartments and in the nucleus of cisplatin-sensitive cells; in the cisplatin-resistant cell line, cisplatin analog **35** remained in the periphery of the cell and was unable to enter the nuclear compartment. In sum, unlike Reedjik and coworkers, Howell *et al.* found the distribution of cisplatin analog **35** to be different between the cisplatin sensitive and resistant cells lines.[123] The disparity between these two results requires further investigation to determine whether the distribution of cisplatin between sensitive and resistant cell lines is truly similar or is cell-line-specific.

Further investigation into the vesicular distribution of cisplatin analog **35** revealed that this compound accumulates within lysosomes. Additionally, elucidation of the role of the Golgi in trafficking of cisplatin analog **35** found cisplatin analog **35** in golgin97-positive vesicles, indicating that cisplatin analog **35** accumulates in the Golgi, where it is then carried throughout the cell, or that it enters these vesicles after they have formed. Similar studies for vesicles of the ATP7A and MRP2 pathways, implicated in cisplatin transport, showed colocalization of cisplatin analog **35**, confirming their role in the transport of cisplatin.[123]

Imaging of platinum species has recently been extended to a mouse model by Weissleder and coworkers using the

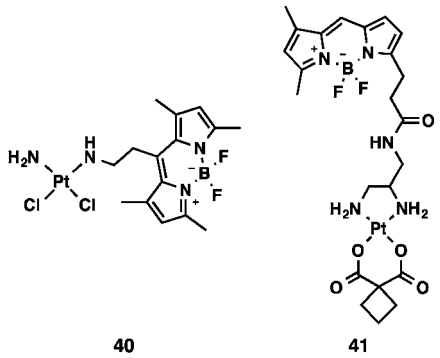

Fig. 31 Compounds used by Weissleder.

BODIPY–cisplatin conjugate **40** or the BODIPY–carboplatin conjugate **41** (Fig. 31) in mice. Incubation of the compounds with OVCA429 and SKOV3 ovarian cancer cells for 48 h determined that the BODIPY–cisplatin conjugate was the most potent compound, while the BODIPY–carboplatin conjugate showed the smallest fold-decrease in potency compared to the parent compound *via* a resazurin-based assay.[124] Imaging studies after incubating OVCA429 cells with 50 μM BODIPY–cisplatin conjugate **40** for 24 h were undertaken and revealed that this conjugate localized to the cytoplasm near the nucleus. To determine whether the BODIPY–cisplatin conjugate **40** was acting in a similar manner as cisplatin (*i.e.* causing DNA damage), colocalization studies using mApple fluorescent protein tagged to 53BP1, a DNA-repair protein localized to the nucleus, were performed. No colocalization with the BODIPY–cisplatin conjugate was observed, likely due to the drug promiscuity inherent in the parent compound. Importantly, this group conducted pharmacokinetic studies on the four compounds; the characteristic short initial half-life followed by longer late half-life of cisplatin was retained in these compounds. Although the compounds had significantly higher log *P* values than the parent compounds, the overall pharmacokinetic profile was similar.

Further, the same group attempted to match pharmacokinetic data with pharmacodynamic data by monitoring DNA damage in tumor cells after treatment with the BODIPY–cisplatin conjugate **40** *via* intravital fluorescence imaging. Mice were treated with **40** and imaged in real time to visualize the distribution of this conjugate and the appearance of mApple puncta. The cisplatin analog appeared diffuse, both in the intra- and extracellular space, with the fluorescence intensity increasing with time (Fig. 32, row 1). A time-dependent increase in the number of mApple puncta was clearly seen after treatment of mice with the BODIPY–cisplatin conjugate **40**, indicating that this analog was generating DNA damage (Fig. 32, rows 2 and 3).[124]

Investigations of cisplatin tagged with Alexa Fluor 546 in cisplatin-sensitive and resistant cell lines were also undertaken.[125] Cisplatin resistant KB-CP.5 and KB-CP20 cells were derived from parental KB-3-1 cells (human KB epidermoid carcinoma). Cells were treated with Alexa Fluor 546-cisplatin conjugate (Molecular Probes) for imaging studies. This conjugate entered cells within minutes, with the highest fluorescence observed in KB-3-1 cells

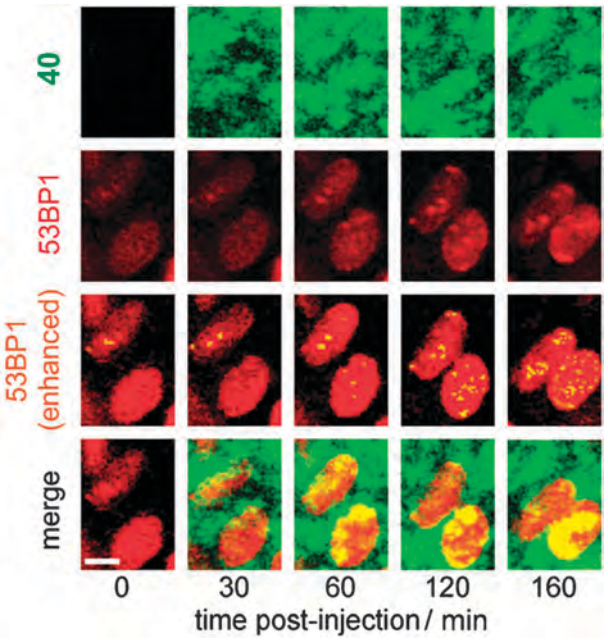

Fig. 32 Zoomed-in image of two tumor cells showing accumulation of 53BP1 puncta over time following treatment with the BODIPY–cisplatin conjugate **40**; scale bar = 5 μm. Adapted with permission from John Wiley and Sons, *ChemMedChem*, 2014, **9**, 1131–1135. Copyright © 2014 Wiley-VCH Verlag GmbH & Co. KGaA, Weinheim.

(Fig. 33, column 1); the fluorescence intensity increased over time. Moderate, time-dependent, fluorescence was observed in KB-CP.5 cells (Fig. 33, column 2); only very weak punctate fluorescence was

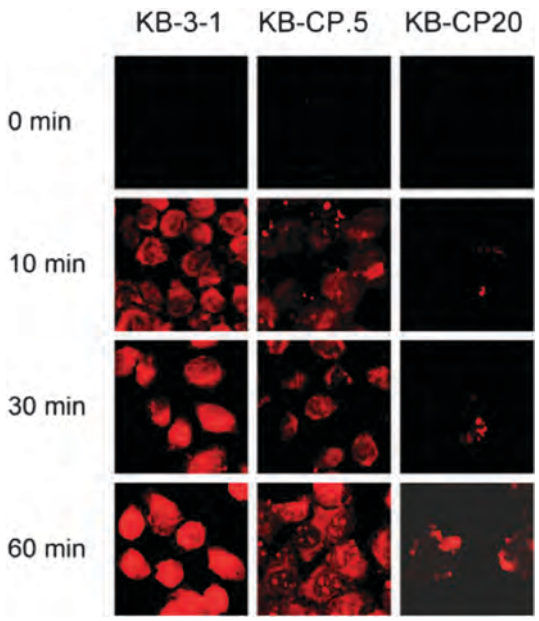

Fig. 33 Fluorescence distribution of Alexa Fluor 546–cisplatin over time in cisplatin-sensitive and resistant KB cells. Fluorescence distribution of Alexa Fluor 546–cisplatin was measured at different times in sensitive parental KB-3-1 cells, single-step cisplatin resistant KB-CP.5 cells, and multi-step selected cisplatin resistant KB-CP20 cells. Adapted with permission from John Wiley and Sons, *J. Cell. Physiol.*, 2005, **202**, 635–641. Copyright © 2005 Wiley-Liss, Inc.

observed in KB-CP20 cells even after 1 h (Fig. 33, column 3). Fluorescence was observed in the nucleus of both KB-3-1 and KB-CP.5 cells, although it was not evenly distributed and appeared to concentrate in the nucleolus in KB-CP.5 cells.

Treatment of cells with the Alexa Fluor 488–cisplatin conjugate (green fluorescent) followed by an antibody for Alexa Fluor 488 was used to determine the distribution of cisplatin complex binding proteins (CCBPs) in the plasma membrane, cytoplasm, and nucleus in KB-3-1 and KB-CP.5 cells. CCBPs were found in lower concentrations in the plasma membrane in KB-CP.5 cells compared to KB-3-1 cells, suggesting that altered trafficking of cisplatin into cells may be a mechanism for cisplatin resistance.

2.3.2 Pt(IV) drugs. Development of the Pt(IV) drug satraplatin has attracted much interest, although FDA approval has yet to be granted. Pt(IV) drugs have the advantage of low toxicity while in the Pt(IV) state, presumably due to the saturated coordination sphere and increased lipophilicity.[89,126] Further, they represent an avenue to circumvent Pt drug resistance. These drugs have the ability to bind to proteins and DNA upon reduction to the Pt(II) state, either intra- or extracellularly.

An investigation into the reduction of Pt(IV) to Pt(II) in cells was attempted by Hambley and coworkers. One of the amines of cisplatin was replaced by coumarin derivatives **42** and **43** to afford Pt(II)-coumarins **44** and **45**, respectively (Fig. 34). Similarly, replacement of one of the amines of a Pt(IV) analog of cisplatin resulted in Pt(IV)-coumarin **46** (Fig. 34); **46** exhibited a lower fluorescence intensity than **44**. It was expected that, intracellularly, Pt(IV)-coumarin **46** would be reduced to Pt(II)-coumarin **44**.[126] These probes were then applied to cells; Pt(II)-trifluorocoumarin **45** was found to be unsuitable for imaging, as the fluorophore dissociated from platinum. A substantial fluorescence intensity from treatment of cells with Pt(IV)-coumarin **46** was observed. The unexpectedly high fluorescence intensity from this compound was attributed to the reduction of Pt(IV)-coumarin **46** to Pt(II)-coumarin **44**. However, the distribution of Pt(II)-coumarin **44** and Pt(IV)-coumarin **46** did not appear to be similar, suggesting that despite the reduction to a Pt(II) compound, the distribution of Pt(IV) compounds display distinct properties from those of Pt(II) compounds. In addition, none of the compounds penetrated the nuclear envelope, although the quenching of fluorescence upon binding to DNA was attributed to this. Colocalization studies with LysoTracker Green showed accumulation of Pt(II)-coumarin **44** in lysosomes. However, previous studies using X-ray imaging did not show cisplatin in these organelles,

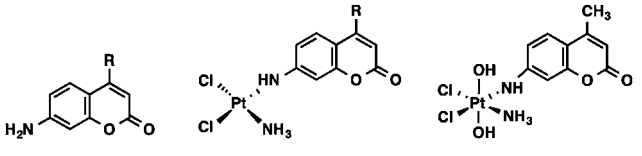

Fig. 34 Compounds used by Hambley and coworkers.

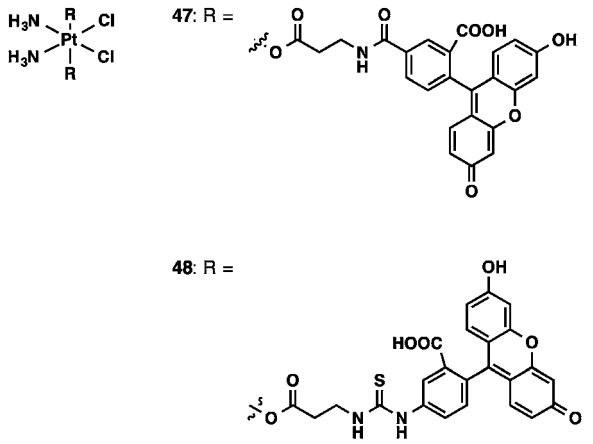

Fig. 35 Compounds developed by Lippard and coworkers.

suggesting that the coumarin affected the distribution of the compound.

A similar system was developed by Lippard and coworkers using fluorescein as the fluorophore. The quantum yield of amide **47** and thiourea **48** (Fig. 35) was 2.5-fold less than that of fluorescein, with quenching occurring by HOMO-FRET and/or possibly heavy metal quenching.[127] These compounds were 10–20-fold less cytotoxic than cisplatin. It was demonstrated that these Pt(IV) compounds would only be reduced to Pt(II) compounds in the presence of biomimetic concentrations of cellular reducing agents, such as glutathione or ascorbate. Further, it was determined that the dissociation of the axial ligands from thiourea **48** was pH-sensitive. Only amide **47** was used for imaging studies.

Treatment with 15 μM amide **47** revealed that fluorescence increased within the cell in 1 h and became stronger and more dispersed over several hours (Fig. 36, column 3). Uptake into the cells continued for 24 h; cotreatment with Hoechst (Fig. 36, column 2) and LysoTracker Red (Fig. 36, column 4) revealed that this amide localized within the lysosomes, as observed by the merged image (Fig. 36, column 5). Treatment with the fluorophore alone showed no intracellular fluorescence, while analysis of the Pt content of DNA saw a Pt-to-base-pair ratio similar to that of cells treated with cisplatin. These data suggest that intact amide **47** enters the cell and releases the axial ligands upon reduction to a Pt(II) compound, whereupon the fluorophore is sequestered in lysosomes while Pt moves to the nucleus to form Pt–DNA adducts. Further analysis of the cell cycle distribution showed an accumulation in S phase 24 h after treatment and an accumulation in G2/M phase after 48 h; these data were comparable to cisplatin. Analysis of the proteins associated with the DNA repair pathway and apoptosis pathways indicated high levels of phosphorylated histone H2AX and cleaved caspases, which correspond to DNA damage from Pt and apoptosis, respectively. It can be concluded that amide **47** sufficiently mimics the properties of cisplatin.

2.3.3 Monofunctional Pt compounds. Several monofunctional Pt compounds have recently attracted interest. These compounds form adducts with DNA that are better able to

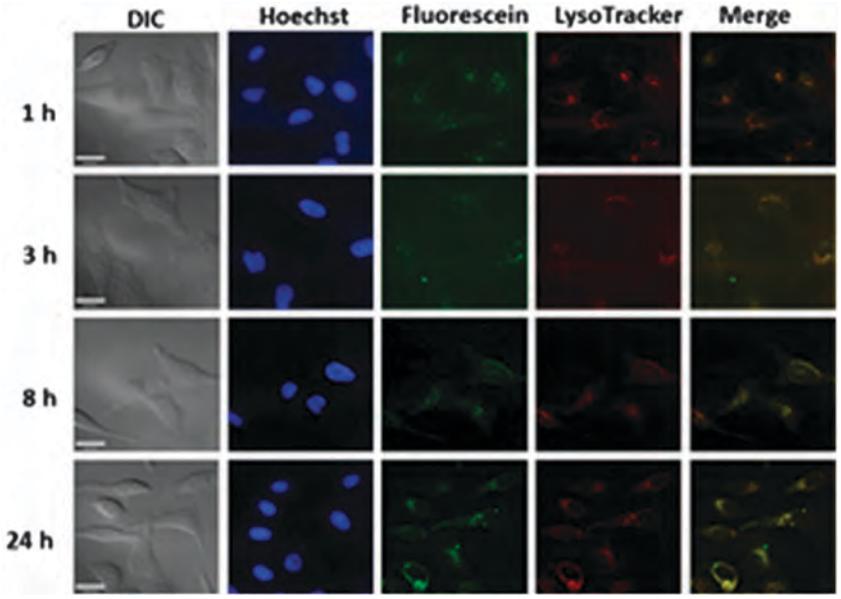

Fig. 36 Differential interference contrast (DIC) and fluorescence images of HeLa cells treated with 15 μM of amide **47** for 1, 3, 8, 24, and 48 h. Scale bar = 26 μm. In addition, cells were incubated with 10 μM Hoechst and 10 μM LysoTracker for 30 min. Reprinted with permission from *Bioconjugate Chem.*, 2013, **24**, 1733–1740. Copyright (2013) American Chemical Society.

evade DNA repair, as well as the ability to inhibit DNA transcription.[128] Little is known about the accumulation and distribution of these drugs; recent studies have attempted to learn more about this class of compounds by fluorescent tagging.

Oxadiazole **49** (Fig. 37) was synthesized to study the cellular accumulation and distribution of monofunctional platinum compounds.[128] Although the oxadiazole was 8-fold less potent than cisplatin, it was able to enter the cell, and most importantly, the nuclear envelope; images of HeLa cells treated with oxadiazole **49** after 10 min are shown in Fig. 38a and c. The uptake of this oxadiazole into cells was slow, only diffusing into the cells after 6 h and only entering the nucleolus after 17 h (Fig. 38b and d); despite this, the ability to enter the nucleolus suggests that Pt–DNA adducts were being formed. The fluorescence intensity within the nucleus decreased over time, suggesting that the cell was repairing the damage caused by this oxadiazole. Further, treatment with the fluorophore alone showed a significantly different distribution than that of the platinum-conjugated fluorophore, suggesting that the Pt center alone could account for the DNA-binding ability.

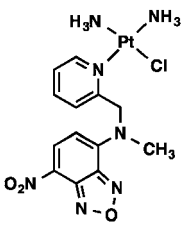

49

Fig. 37 Compound developed by Guo and Wang.

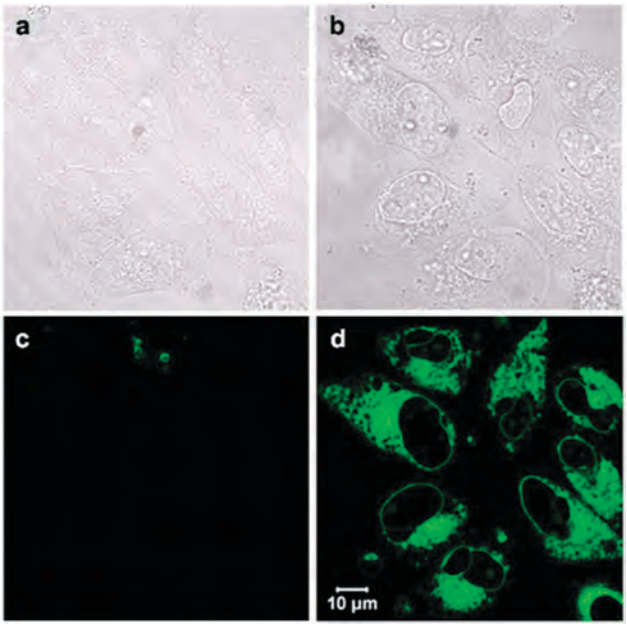

Fig. 38 Phase contrast images (a, b) and corresponding fluorescent images of HeLa cells after incubation with 10 μM oxadiazole **49** for 10 min (a, c) and 17 h (b, d), respectively (λ_{ex} = 488 nm). Adapted from *Dalton Trans.*, 2011, **40**, 10376 with permission of The Royal Society of Chemistry.

2.3.4 Intercalators and Pt. One of the most potent sets of drugs to be developed has involved the conjugation of intercalators to Pt. These compounds are capable of forming Pt–DNA adducts, while simultaneously inserting into DNA. Several intercalators are inherently fluorescent, but binding to Pt may result in fluorescence quenching.[129–132]

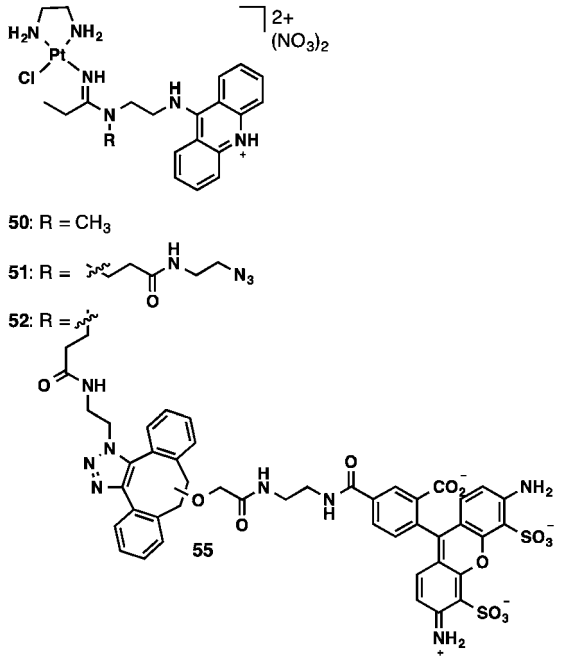

Fig. 39 Compounds used by Bierbach and coworkers.

The Bierbach group recently recognized the drawbacks of conjugating fluorophores to Pt-drugs, namely that they may interfere with the drugs' mechanism of action. They hypothesized that post-labeling would allow for accurate imaging of the drug without interfering with its action. In their investigation of Pt-drug **50** (Fig. 39), they found that many linkers interfered with the compound's ability to interact with DNA. Eventually, azide **51** (Fig. 39) was synthesized, which was able to undergo click chemistry with Alexa Fluor 488 alkyne.

After verification that azide **51** was bound to DNA *via* Pt adducts, this azide was applied towards cellular imaging in NCI-H460 cells in conjunction with Hoechst 33342. Cells were fixed prior to the addition of the click reaction mixture. Control cells were treated with only the copper-based reaction buffer containing Alexa Fluor 488 alkyne; no green fluorescence corresponding to the Alexa Fluor 488 was observed (Fig. 40a). Images corresponding to Hoechst staining (Fig. 40b), the merge of the Hoechst and Alexa Fluor 488 (Fig. 40c), and the bright-field image (Fig. 40d) were also shown. Incubation of cells with azide **51**, followed by the addition of the click reaction buffer without copper yielded similar results as the control (Fig. 40e–h). Cells treated with azide **51**, Alexa Fluor 488 alkyne, and $CuSO_4$ revealed green fluorescence in the nucleus (Fig. 40i) that colocalized with Hoechst (Fig. 40j and k).

Further studies by this group attempted to develop a copper-free post-labeling technique and to compare the effects of pre- and post-labeling.[133] Attempts to develop a copper-free post-labeling technique met with many challenges, including high background fluorescence and the inability to label the Pt-adducts in DNA of dividing cells due to the steric bulk of the fluorescent tag, and were ultimately abandoned. Several compounds were used to investigate the effects of pre-labeling. Red-fluorescent Alexa Fluor 647 alkyne was reacted with azide **51** as the post-labeling sample. Rhodamine-derivative **52** (Fig. 39, green fluorescent) served as the

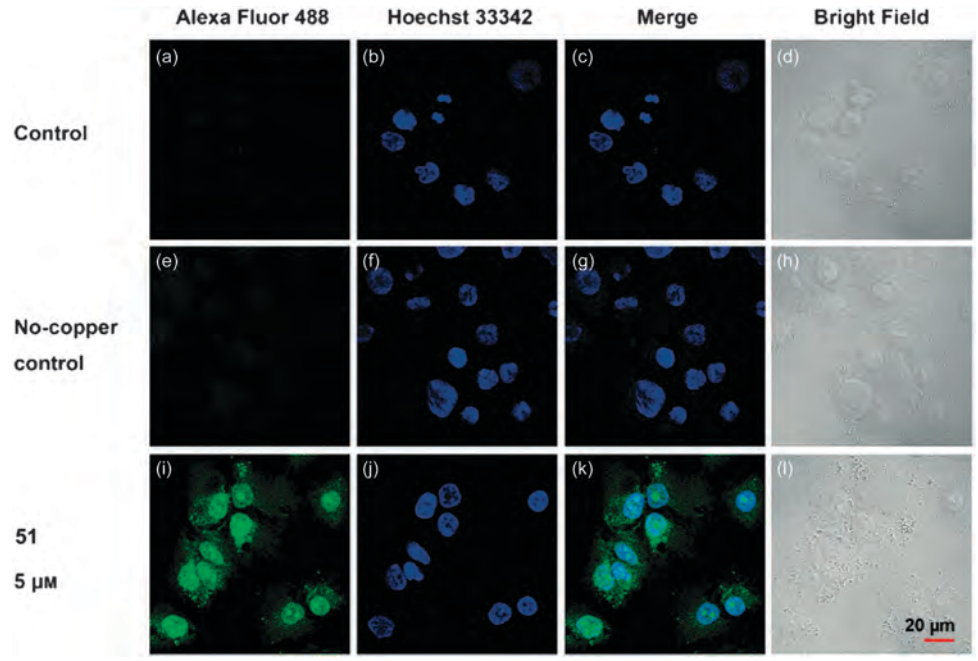

Fig. 40 Imaging of 5 μM **51** in fixed NCI-H460 lung cancer cells using Alexa Fluor 488-alkyne. Cells were co-stained with Hoechst 33342. Single confocal image planes of Alexa Fluor 488 (green), Hoechst 33342 (blue), the green and blue channels merged, and corresponding bright field image are shown for azide **51** treatment and control conditions. The control group was treated with Alexa Fluor 488-alkyne and copper-based ligation buffer. The no-copper control was treated with Alexa Fluor 488-alkyne in the absence of copper ions. Adapted with permission from John Wiley and Sons, *Angew. Chem.*, 2013, **125**, 3434–3438. Copyright © 2013 Wiley-VCH Verlag GmbH & Co. KGaA, Weinheim.

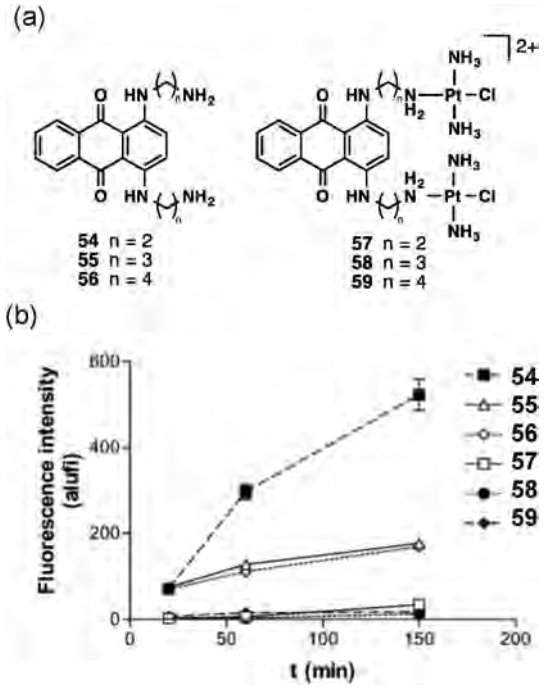

Fig. 41 (a) Structures of compounds used by Reedijk leading to *in vitro* imaging. (b) Quantification of the mean fluorescence intensity per pixel inside A2780 cells as determined digitally from the fluorescence microscopic images. Fluorescence intensity is given in alufi (arbitrary units of fluorescence intensity). Adapted from *JBIC, J. Biol. Inorg. Chem.*, 2004, **9**, 403–413. With kind permission from Springer Science and Business Media.

pre-labeling sample. NCI-H460 cells were then simultaneously treated with azide **51** and rhodamine derivative **52**. Azide **51** and rhodamine derivative **52** mostly colocalized throughout the cell, but more intense fluorescence was observed from azide **51** in chromatin, suggesting that the size of the rhodamine derivative may have affected its ability to bind to DNA. The post-labeling technique was then used to monitor DNA and RNA synthesis in cells treated with azide **51**, finding that DNA/RNA synthesis is severely retarded in cells treated with this azide.

A second type of Pt-intercalator complex was developed by Reedijk and coworkers, who used the inherent fluorescence of the intercalators to monitor the drugs' distribution throughout the cell. In these complexes, two cisplatin derivatives were conjugated to a single intercalator using linkers of varying lengths.[130–132] In human ovarian cancer A2780 cells and their cisplatin-resistant counterpart, A2780cisR, comparison of diaminoanthracene derivatives **54–56** (Fig. 41a) found that longer linkers interfered with cell uptake as measured by fluorescence intensity (Fig. 41b); the same trend held for the platinated analogs **57–59**. The fluorescence from the platinated analogs was substantially lower than that of the nonplatinated diaminoanthracene-derivatives.

The distributions of diaminoanthracene derivatives **54–59** in A2780 cells were largely the same, with the exception that in cells treated with the platinated diaminoanthracene derivatives fluorescence was not detected in the nucleus even after 24 h and that fluorescence appeared in vesicles after 24 h. The lack of fluorescence in the nucleus was attributed to quenching by DNA upon intercalation. This was confirmed by UV and FAAS methods; further, it was found that there was a higher Pt-to-base-pair ratio in cells treated with **57** than in cisplatin treated cells. Colocalization studies with LysoTracker found that the vesicles that exhibited fluorescence were lysosomes.

However, the distribution of platinated diaminoanthracene derivatives **57–59** in A2780 differed compared to their distribution in A2780cisR. Fluorescence was observed in lysosomes after 20 min incubation with **57**, whereas this same event occurred only after 24 h in the nonresistant line.[131] It was later determined that lysosomes of A2780cisR cells had a higher pH, which accounts for the rapid uptake of **57** into lysosomes.[132]

2.4 Conclusions

In conclusion, significant progress has been made using fluorescence spectroscopy to understand the mode of action of platinum drugs. Although direct platinum detection techniques have yet to be applied to cellular imaging, the development of selective platinum probes will allow for bioorthogonal determination of the distribution and trafficking of platinum drugs throughout the cell. Further, quantitative high throughput methods are needed to facilitate pharmacokinetic studies in clinical studies and personalized chemotherapy with platinum drugs in the clinic. Fluorescent tagging of platinum drugs has been applied to many compounds and cell lines, yielding much insight into the distribution and trafficking of these drugs. However, caution must be used with methods that fluorescently tagged Pt-drugs. A study that attempted to verify that fluorescently-tagged Pt-drugs showed the same distribution as cisplatin *via* platinum-mapping using X-ray fluorescence computed micro-tomography and X-ray fluorescence microscopy in DLD-1 spheroids found that the fluorophore dissociated from the complex and localized to the surface of the spheroids, while the Pt migrated towards the center.[134] Despite this, much knowledge has been gained from these types of studies, such as insight to mechanisms of resistance and distribution of drugs throughout the cell. Developments in this field will allow for the design of new types of platinum drugs. Additionally, platinum-based fuel cells are being developed, which requires the quality control of the material over time to monitor platinum leaching. Applications of chemosensors in energy science may elucidate the mechanism of material degradation and distribution of platinum on electrodes.

Acknowledgements

This work was in part supported by the US National Science Foundation (Grant CHE-0911092).

References

1 K. C. Nicolaou, P. G. Bulger and D. Sarlah, *Angew. Chem., Int. Ed.*, 2005, **44**, 4442–4489.
2 J. S. Carey, D. Laffan, C. Thomson and M. T. Williams, *Org. Biomol. Chem.*, 2006, **4**, 2337–2347.

3 S. V. Chankeshwara, E. Indrigo and M. Bradley, *Curr. Opin. Chem. Biol.*, 2014, **21C**, 128–135.
4 C. E. I. Knappke and A. Jacobi von Wangelin, *Chem. Soc. Rev.*, 2011, **40**, 4948–4962.
5 N. Miyaura and A. Suzuki, *Chem. Rev.*, 1995, **95**, 2457–2483.
6 A. O. King, N. Okukado and E. I. Negishi, *J. Chem. Soc., Chem. Commun.*, 1977, 683–684.
7 D. Mc Cartney and P. J. Guiry, *Chem. Soc. Rev.*, 2011, **40**, 5122–5150.
8 R. Chinchilla and C. Najera, *Chem. Rev.*, 2007, **107**, 874–922.
9 D. S. Surry and S. L. Buchwald, *Chem. Sci.*, 2011, **2**, 27–50.
10 P. Espinet and A. M. Echavarren, *Angew. Chem., Int. Ed.*, 2004, **43**, 4704–4734.
11 B. M. Trost and M. L. Crawley, *Chem. Rev.*, 2003, **103**, 2921–2944.
12 K. S. Chan, M. Wasa, L. Chu, B. N. Laforteza, M. Miura and J. Q. Yu, *Nat. Chem.*, 2014, **6**, 146–150.
13 J. D. Zhang, A. Bellomo, A. D. Creamer, S. D. Dreher and P. J. Walsh, *J. Am. Chem. Soc.*, 2012, **134**, 13765–13772.
14 F. Palazzo, S. Giovagnoli, A. Schoubben, P. Blasi, C. Rossi and M. Ricci, *Int. J. Pharm.*, 2013, **440**, 273–282.
15 J. T. Hou, K. Li, K. K. Yu, M. Z. Ao, X. Wang and X. Q. Yu, *Analyst*, 2013, **138**, 6632–6638.
16 L. P. Duan, Y. F. Xu and X. H. Qian, *Chem. Commun.*, 2008, 6339–6341.
17 R. J. T. Houk, K. J. Wallace, H. S. Hewage and E. V. Anslyn, *Tetrahedron*, 2008, **64**, 8271–8278.
18 K. T. Nielsen, K. Bechgaard and F. C. Krebs, *Synthesis*, 2006, 1639–1644.
19 B. Tang, H. Zhang and Y. Wang, *Anal. Lett.*, 2004, **37**, 1219–1231.
20 K. J. Wallace, *Supramol. Chem.*, 2009, **21**, 89–102.
21 M. S. Baker and S. T. Phillips, *J. Am. Chem. Soc.*, 2011, **133**, 5170–5173.
22 J. Jiang, H. E. Jiang, W. Liu, X. L. Tang, X. Zhou, R. T. Liu and W. S. Liu, *Org. Lett.*, 2011, **13**, 4922–4925.
23 H. Kim, K. S. Moon, S. Shim and J. Tae, *Chem. – Asian J.*, 2011, **6**, 1987–1991.
24 H. Mohapatra and S. T. Phillips, *Anal. Chem.*, 2012, **84**, 8927–8931.
25 H. Mohapatra, K. M. Schmid and S. T. Phillips, *Chem. Commun.*, 2012, **48**, 3018–3020.
26 S. Mukherjee, S. Chowdhury, A. K. Paul and R. Banerjee, *J. Lumin.*, 2011, **131**, 2342–2346.
27 E. Pershagen, J. Nordholm and K. E. Borbas, *J. Am. Chem. Soc.*, 2012, **134**, 9832–9835.
28 W. X. Ren, T. Pradhan, Z. Yang, Q. Y. Cao and J. S. Kim, *Sens. Actuators, B*, 2012, **171**, 1277–1282.
29 S. y. Yu, H.-W. Rhee and J.-I. Hong, *Tetrahedron Lett.*, 2011, **52**, 1512–1514.
30 M. E. Jun and K. H. Ahn, *Org. Lett.*, 2010, **12**, 2790–2793.
31 S. Y. Ahn, S. Kim, K. Baek, M. S. Eom, S. Kang and M. S. Han, *Bull. Korean Chem. Soc.*, 2014, **35**, 2189–2192.
32 R. Balamurugan, C. C. Chien, K. M. Wu, Y. H. Chiu and J. H. Liu, *Analyst*, 2013, **138**, 1564–1569.
33 X. D. Bu, K. Koide, E. J. Carder and C. J. Welch, *Org. Process Res. Dev.*, 2013, **17**, 108–113.
34 S. T. Cai, Y. Lu, S. He, F. F. Wei, L. C. Zhao and X. S. Zeng, *Chem. Commun.*, 2013, **49**, 822–824.
35 L. Cui, W. P. Zhu, Y. F. Xu and X. H. Qian, *Anal. Chim. Acta*, 2013, **786**, 139–145.
36 A. L. Garner and K. Koide, *J. Am. Chem. Soc.*, 2008, **130**, 16472–16473.
37 A. L. Garner and K. Koide, *Chem. Commun.*, 2009, 86–88.
38 A. L. Garner, F. L. Song and K. Koide, *J. Am. Chem. Soc.*, 2009, **131**, 5163–5171.
39 S. Goswami, A. Manna, A. K. Maity, S. Paul, A. K. Das, M. K. Das, P. Saha, C. K. Quah and H. K. Fun, *Dalton Trans.*, 2013, **42**, 12844–12848.
40 K. Inamoto, L. D. Campbell, T. Doi and K. Koide, *Tetrahedron Lett.*, 2012, **53**, 3147–3148.
41 D. Keum, S. Kim and Y. Kim, *Chem. Commun.*, 2014, **50**, 1268–1270.
42 F. L. Song, E. J. Carder, C. C. Kohler and K. Koide, *Chem. – Eur. J.*, 2010, **16**, 13500–13508.
43 F. L. Song, A. L. Garner and K. Koide, *J. Am. Chem. Soc.*, 2007, **129**, 12354–12355.
44 H. L. Li, J. L. Fan, J. J. Du, K. X. Guo, S. G. Sun, X. J. Liu and X. J. Peng, *Chem. Commun.*, 2010, **46**, 1079–1081.
45 H. L. Li, J. L. Fan, M. M. Hu, G. H. Cheng, D. H. Zhou, T. Wu, F. L. Song, S. G. Sun, C. Y. Duan and X. J. Peng, *Chem. – Eur. J.*, 2012, **18**, 12242–12250.
46 H. L. Li, J. L. Fan, X. J. Liu, S. G. Sun and X. J. Peng, *Chem. J. Chin. Univ.*, 2010, **31**, 1725–1728.
47 B. Liu, Y. Bao, F. Du, H. Wang, J. Tian and R. Bai, *Chem. Commun.*, 2011, **47**, 1731–1733.
48 B. Liu, Y. Y. Bao, H. Wang, F. F. Du, J. Tian, Q. B. Li, T. S. Wang and R. K. Bai, *J. Mater. Chem.*, 2012, **22**, 3555–3561.
49 B. Liu, H. G. Dai, Y. Y. Bao, F. F. Du, J. Tian and R. K. Bai, *Polym. Chem.*, 2011, **2**, 1699–1705.
50 B. Liu, H. Wang, T. S. Wang, Y. Y. Bao, F. F. Du, J. Tian, Q. B. A. Li and R. K. Bai, *Chem. Commun.*, 2012, **48**, 2867–2869.
51 J. P. Li, H. X. Wang, H. X. Wang, M. S. Xie, G. R. Qu, H. Y. Niu and H. M. Guo, *Eur. J. Org. Chem.*, 2014, 2225–2230.
52 Y. X. Wang, B. Liu, J. Tian, Q. B. A. Li, F. F. Du, T. S. Wang and R. K. Bai, *Analyst*, 2013, **138**, 779–782.
53 Z. Wang and F. Liao, *Synth. Met.*, 2012, **162**, 444–447.
54 Z. Wang, S. Zheng, J. Cai, P. Wang, J. Feng, X. Yang, L. Zhang, M. Ji, F. Wu, N. He and N. Wan, *Anal. Chem.*, 2013, **85**, 11602–11609.
55 J. He, M. Zha, J. Cui, M. Zeller, A. D. Hunter, S. M. Yiu, S. T. Lee and Z. Xu, *J. Am. Chem. Soc.*, 2013, **135**, 7807–7810.
56 Y. Wang, B. Liu, J. Tian, Q. Li, F. Du, T. Wang and R. Bai, *Analyst*, 2013, **138**, 779–782.
57 Z. Wang, S. Zheng, J. Cai, P. Wang, J. Feng, X. Yang, L. Zhang, M. Ji, F. Wu, N. He and N. Wan, *Anal. Chem.*, 2013, **85**, 11602–11609.
58 H. L. Li, J. F. Cao, H. Zhu, J. L. Fan and X. J. Peng, *Tetrahedron Lett.*, 2013, **54**, 4357–4361.

59 D. K. Prusty, M. Kwak, J. Wildeman and A. Herrmann, *Angew. Chem., Int. Ed.*, 2012, **51**, 11894–11898.
60 R. M. Yusop, A. Unciti-Broceta, E. M. V. Johansson, R. M. Sanchez-Martin and M. Bradley, *Nat. Chem.*, 2011, **3**, 239–243.
61 J. Li, S. X. Lin, J. Wang, S. Jia, M. Y. Yang, Z. Y. Hao, X. Y. Zhang and P. R. Chen, *J. Am. Chem. Soc.*, 2013, **135**, 7330–7338.
62 N. Li, R. K. V. Lim, S. Edwardraja and Q. Lin, *J. Am. Chem. Soc.*, 2011, **133**, 15316–15319.
63 A. E. Speers, G. C. Adam and B. F. Cravatt, *J. Am. Chem. Soc.*, 2003, **125**, 4686–4687.
64 D. C. Kennedy, R. K. Lyn and J. P. Pezacki, *J. Am. Chem. Soc.*, 2009, **131**, 2444–2445.
65 M. Santra, S. K. Ko, I. Shin and K. H. Ahn, *Chem. Commun.*, 2010, **46**, 3964–3966.
66 B. C. Zhu, C. C. Gao, Y. Z. Zhao, C. Y. Liu, Y. M. Li, Q. Wei, Z. M. Ma, B. Du and X. L. Zhang, *Chem. Commun.*, 2011, **47**, 8656–8658.
67 W. Liu, J. Jiang, C. Chen, X. Tang, J. Shi, P. Zhang, K. Zhang, Z. Li, W. Dou, L. Yang and W. Liu, *Inorg. Chem.*, 2014, **53**, 12590–12594.
68 J. L. Zhang, L. Zhang, Y. M. Zhou, T. S. Ma and J. Y. Niu, *Microchim. Acta*, 2013, **180**, 211–217.
69 P. Kaur, N. Kaur, M. Kaur, V. Dhuna, J. Singh and K. Singh, *RSC Adv.*, 2014, **4**, 16104–16108.
70 D. Li, L. D. Campbell, B. A. Austin and K. Koide, *ChemPlusChem*, 2012, **77**, 281–283.
71 J. M. Williams and K. Koide, *Ind. Eng. Chem. Res.*, 2013, **52**, 8612–8615.
72 C. Streu and E. Meggers, *Angew. Chem., Int. Ed.*, 2006, **45**, 5645–5648.
73 J. T. Weiss, J. C. Dawson, K. G. Macleod, W. Rybski, C. Fraser, C. Torres-Sanchez, E. E. Patton, M. Bradley, N. O. Carragher and A. Unciti-Broceta, *Nat. Commun.*, 2014, **5**, 3277.
74 K. Koide, F. Song, E. D. de Groh, A. L. Garner, V. D. Mitchell, L. A. Davidson and N. A. Hukriede, *ChemBioChem*, 2008, **9**, 214–218.
75 R. A. Smith, C. M. Porteous, A. M. Gane and M. P. Murphy, *Proc. Natl. Acad. Sci. U. S. A.*, 2003, **100**, 5407–5412.
76 C. D. Spicer, T. Triemer and B. G. Davis, *J. Am. Chem. Soc.*, 2012, **134**, 800–803.
77 X. Ma, H. Wang and W. Chen, *J. Org. Chem.*, 2014, **79**, 8652–8658.
78 B. W. Michel, A. R. Lippert and C. J. Chang, *J. Am. Chem. Soc.*, 2012, **134**, 15668–15671.
79 L. Yuan, W. Y. Lin, K. B. Zheng, L. W. He and W. M. Huang, *Chem. Soc. Rev.*, 2013, **42**, 622–661.
80 H. Chen, W. Y. Lin and L. Yuan, *Org. Biomol. Chem.*, 2013, **11**, 1938–1941.
81 X. Wang, Z. Guo, S. Zhu, H. Tian and W. Zhu, *Chem. Commun.*, 2014, **50**, 13525–13528.
82 M. Akaboshi, K. Kawai, Y. Tanaka, J. Takada and N. Fujii, *Biol. Trace Elem. Res.*, 1999, **71–72**, 585–593.
83 M. E. Bosch, A. J. R. Sanchez, F. S. Rojas and C. B. Ojeda, *J. Pharm. Biomed. Anal.*, 2008, **47**, 451–459.
84 S. Dhar, F. X. Gu, R. Langer, O. C. Farokhzad and S. J. Lippard, *Proc. Natl. Acad. Sci. U. S. A.*, 2008, **105**, 17356–17361.
85 P. J. Dyson and G. Sava, *Dalton Trans.*, 2006, 1929–1933.
86 D. P. Gately and S. B. Howell, *Br. J. Cancer*, 1993, **67**, 1171–1176.
87 E. R. Jamieson and S. J. Lippard, *Chem. Rev.*, 1999, **99**, 2467–2498.
88 I. W. H. Jarvis, E. L. Meczes, H. D. Thomas, R. J. Edmondson, G. J. Veal, A. V. Boddy, C. J. Ottley, D. G. Pearson and M. J. Tilby, *Biochem. Pharmacol.*, 2012, **83**, 69–77.
89 A. V. Klein and T. W. Hambley, *Chem. Rev.*, 2009, **109**, 4911–4920.
90 S. Marnitz, C. Kohler, P. Oppelt, A. Schmittel, G. Favero, K. Hasenbein, A. Schneider and M. Markman, *Oncology*, 2010, **79**, 72–77.
91 M. F. Osborn, J. D. White, M. M. Haley and V. J. DeRose, *ACS Chem. Biol.*, 2014, **9**, 2404–2411.
92 M. J. Egorin, D. A. Van Echo, E. A. Olman, M. Y. Whitacre, A. Forrest and J. Aisner, *Cancer Res.*, 1985, **45**, 6502–6506.
93 S. Benezet, R. Guimbaud, E. Chatelut, C. Chevreau, R. Bugat and P. Canal, *Ann. Oncol.*, 1997, **8**, 607–609.
94 E. Chatelut, P. Canal, V. Brunner, C. Chevreau, A. Pujol, A. Boneu, H. Roche, G. Houin and R. Bugat, *J. Natl. Cancer Inst.*, 1995, **87**, 573–580.
95 M. J. Egorin, D. A. Van Echo, S. J. Tipping, E. A. Olman, M. Y. Whitacre, B. W. Thompson and J. Aisner, *Cancer Res.*, 1984, **44**, 5432–5438.
96 A. Schmitt, L. Gladieff, A. Lansiaux, C. Bobin-Dubigeon, M. C. Etienne-Grimaldi, M. Boisdron-Celle, F. Serre-Debauvais, F. Pinguet, A. Floquet, E. Billaud, C. Le Guellec, N. Penel, M. Campone, R. Largillier, O. Capitain, M. Fabbro, N. Houede, J. Medioni, P. Bougnoux, I. Lochon and E. Chatelut, *Clin. Cancer Res.*, 2009, **15**, 3633–3639.
97 F. Thomas, S. Seronie-Vivien, L. Gladieff, F. Dalenc, V. Durrand, L. Mallard, T. Lafont, M. Poublanc, R. Bugat and E. Chatelut, *Clin. Pharmacokinet.*, 2005, **44**, 1305–1316.
98 A. H. Calvert, D. R. Newell, L. A. Gumbrell, S. Oreilly, M. Burnell, F. E. Boxall, Z. H. Siddik, I. R. Judson, M. E. Gore and E. Wiltshaw, *J. Clin. Oncol.*, 1989, **7**, 1748–1756.
99 E. Reed, R. F. Ozols, R. Tarone, S. H. Yuspa and M. C. Poirier, *Carcinogenesis*, 1988, **9**, 1909–1911.
100 J. H. Schellens, J. Ma, A. S. Planting, M. E. van der Burg, E. van Meerten, M. de Boer-Dennert, P. I. Schmitz, G. Stoter and J. Verweij, *Br. J. Cancer*, 1996, **73**, 1569–1575.
101 F. E. de Jongh, J. Verweij, W. J. Loos, R. de Wit, M. J. de Jonge, A. S. Planting, K. Nooter, G. Stoter and A. Sparreboom, *J. Clin. Oncol.*, 2001, **19**, 3733–3739.
102 Y. Yamada, Y. Ikuta, K. Nosaka, N. Miyanari, N. Hayashi, H. Mitsuya and H. Baba, *Case Rep. Med.*, 2010, **2010**, 802312.
103 J. Choi, J. C. Oh, K. H. Kim, S. Y. Chong, M. S. Kang and D. Oh, *Yonsei Med. J.*, 2002, **43**, 128–132.
104 G. Chu, R. Mantin, Y. M. Shen, G. Baskett and H. Sussman, *Cancer*, 1993, **72**, 3707–3714.

105 J. L. Lagrange, E. Cassuto-Viguier, V. Barbe, J. L. Fischel, J. R. Mondain, M. C. Etienne, J. M. Ferrero, A. Creisson-Ducray, P. Formento and G. Milano, *Eur. J. Cancer*, 1994, **30A**, 2057–2060.
106 G. Hofmann, T. Bauernhofer, P. Krippl, D. Lang-Loidolt, S. Horn, W. Goessler, W. Schippinger, F. Ploner, H. Stoeger and H. Samonigg, *BMC Cancer*, 2006, **6**, 1.
107 C. Charlier, P. Kintz, N. Dubois and G. Plomteux, *J. Anal. Toxicol.*, 2004, **28**, 138–140.
108 T. Jurek, M. Rorat, P. Dys and B. Swiatek, *Onkologie*, 2013, **36**, 49–52.
109 X. Pourrat, D. Antier, I. Crenn, G. Calais, A. P. Jonville-Bera and A. Rouleau, *Pharm. World Sci.*, 2004, **26**, 64–65.
110 F. Brivet, J. M. Pavlovitch, A. Gouyette, M. L. Cerrina, G. Tchernia and J. Dormont, *Cancer Chemother. Pharmacol.*, 1986, **18**, 183–184.
111 B. Erdlenbruch, A. Pekrun, H. Schiffmann, O. Witt and M. Lakomek, *Med. Pediatr. Oncol.*, 2002, **38**, 349–352.
112 B. J. Katz, J. H. Ward, K. B. Digre, D. J. Creel and N. Mamalis, *J. Neuroophthalmol.*, 2003, **23**, 132–135.
113 E. Vila-Torres, A. Albert-Mari, D. Almenar-Cubells and N. V. Jimenez-Torres, *J. Oncol. Pharm. Pract.*, 2009, **15**, 249–253.
114 D. SheikhHamad, K. Timmins and Z. Jalali, *J. Am. Soc. Nephrol.*, 1997, **8**, 1640–1644.
115 R. Y. Tsang, T. Al-Fayea and H. J. Au, *Drug Saf.*, 2009, **32**, 1109–1122.
116 N. Nishiyama, S. Okazaki, H. Cabral, M. Miyamoto, Y. Kato, Y. Sugiyama, K. Nishio, Y. Matsumura and K. Kataoka, *Cancer Res.*, 2003, **63**, 8977–8983.
117 D. E. Ryan, *Analyst*, 1951, **76**, 167–171.
118 A. L. Garner and K. Koide, *Chem. Commun.*, 2009, 83–85.
119 B. Ahn, J. Park, K. Singha, H. Park and W. J. Kim, *J. Mater. Chem. B*, 2013, **1**, 2829–2836.
120 H. Kim, S. Lee, J. Lee and J. Tae, *Org. Lett.*, 2010, **12**, 5342–5345.
121 D. Montagner, S. Q. Yap and W. H. Ang, *Angew. Chem., Int. Ed.*, 2013, **52**, 11785–11789.
122 C. Molenaar, J. M. Teuben, R. J. Heetebrij, H. J. Tanke and J. Reedijk, *JBIC, J. Biol. Inorg. Chem.*, 2000, **5**, 655–665.
123 R. Safaei, K. Katano, B. J. Larson, G. Samimi, A. K. Holzer, W. Naerdemann, M. Tomioka, M. Goodman and S. B. Howell, *Clin. Cancer Res.*, 2005, **11**, 756–767.
124 M. A. Miller, B. Askevold, K. S. Yang, R. H. Kohler and R. Weissleder, *ChemMedChem*, 2014, **9**, 1131–1135.
125 X. J. Liang, D. W. Shen, K. G. Chen, S. M. Wincovitch, S. H. Garfield and M. M. Gottesman, *J. Cell. Physiol.*, 2005, **202**, 635–641.
126 E. J. New, R. Duan, J. Z. Zhang and T. W. Hambley, *Dalton Trans.*, 2009, 3092–3101.
127 Y. Song, K. Suntharalingam, J. S. Yeung, M. Royzen and S. J. Lippard, *Bioconjugate Chem.*, 2013, **24**, 1733–1740.
128 S. Wu, X. Wang, C. Zhu, Y. Song, J. Wang, Y. Li and Z. Guo, *Dalton Trans.*, 2011, **40**, 10376–10382.
129 S. Ding, X. Qiao, J. Suryadi, G. S. Marrs, G. L. Kucera and U. Bierbach, *Angew. Chem., Int. Ed.*, 2013, **52**, 3350–3354.
130 B. A. Jansen, P. Wielaard, G. V. Kalayda, M. Ferrari, C. Molenaar, H. J. Tanke, J. Brouwer and J. Reedijk, *JBIC, J. Biol. Inorg. Chem.*, 2004, **9**, 403–413.
131 G. V. Kalayda, B. A. Jansen, C. Molenaar, P. Wielaard, H. J. Tanke and J. Reedijk, *JBIC, J. Biol. Inorg. Chem.*, 2004, **9**, 414–422.
132 G. V. Kalayda, B. A. Jansen, P. Wielaard, H. J. Tanke and J. Reedijk, *JBIC, J. Biol. Inorg. Chem.*, 2005, **10**, 305–315.
133 X. Qiao, S. Ding, F. Liu, G. L. Kucera and U. Bierbach, *JBIC, J. Biol. Inorg. Chem.*, 2014, **19**, 415–426.
134 J. Z. Zhang, N. S. Bryce, A. Lanzirotti, C. K. Chen, D. Paterson, M. D. de Jonge, D. L. Howard and T. W. Hambley, *Metallomics*, 2012, **4**, 1209–1217.